An open-source model and solution method to predict co-contraction in the index finger

An open-source musculoskeletal model and EMG-constrained static optimization solution method to predict co-contraction in the index finger

By

Alexander MacIntosh, B.Sc.

A Thesis Submitted to the School of Graduate Studies in

Partial Fulfillment of the Requirements for the Degree

Master of Science

McMaster University

MASTER OF SCIENCE (2014) McMaster University

(Kinesiology) Hamilton, Ontario

TITLE: An open-source musculoskeletal model and EMG-constrained static optimization solution method to predict co-contraction in the index finger

AUTHOR: Alexander MacIntosh, B.Sc. (University of Waterloo)

SUPERVISOR: Dr. Peter J. Keir

NUMBER OF PAGES: x, 100

ABSTRACT

Determining tendon tension in the finger is essential to understanding forces that may be detrimental to hand function. Direct measurement is not feasible, making biomechanical modelling the best way to estimate these forces. In this study, the intrinsic muscles and extensor mechanism were added to an existing model of the index finger, and as such, it has been named the Intrinsic model. The Intrinsic model of the index finger has 4 degrees of freedom and 7 muscles (with 14 components). Muscle properties and paths for all extrinsic and intrinsic muscles were derived from the literature. Two models were evaluated, the Intrinsic model and the model it was adapted from (identified in this thesis as the Extrinsic-only model). To complement the model, multiple static optimization solution methods were also developed that allowed for EMG-constrained solutions and applied objective functions to promote co-contraction. To test the models and solution methods, 10 participants performed 9 static pressing tasks at 3 force levels, and 5 free motion dynamic tasks at 2 speeds. Kinematics, contact forces, and EMG (from the extrinsic muscles and first dorsal interosseous) were collected. For all solution methods, muscle activity predicted using the Intrinsic model was compared to activity from the model currently available through open-source software (OpenSim). Just by using the Intrinsic model, co-contraction increased by 16% during static palmar pressing tasks. The EMG-constrained solution methods gave a smaller difference between predicted and experimental activity compared to the optimization-only approach ($p < 0.03$). The model and solution methods developed in this thesis improve co-contraction and tendon tension estimates in the finger. As such, this work contributes to our understanding of the control of the hand and the forces that may be detrimental to hand function.

ACKNOWLEDGMENTS

Many thanks go to Dr. Peter Keir for helping me to discover this field. You have allowed me to pursue an area of great interest to me, and while doing so, you framed our work in a more broad and useful context. I now feel confident in applying this work to any project that I may have in the future. Personally, I feel this is very important. I would like to acknowledge my committee members, Dr. Jim Potvin and Dr. Aimee Nelson. I place great weight in your comments. Your contributions are instrumental to the quality of this research, and I appreciate your time towards my work. Thanks to everyone in the lab for letting me bounce ideas off of you. It was a terrific environment to discuss mechanical theory as well as working through technical problems. I am extremely grateful to Tyler Szepesi, who allowed me to use his expert programming skill to quickly realize the Analysis tool plugin. Finally, I would like to thank my family. I receive great strength from those close to me. You are my reason for balance, my reminder of perspective, and my source of determination. Thank you.

TABLE OF CONTENTS

LIST OF TABLES

LIST OF FIGURES

LIST OF ABBREVIATIONS

Central slip	cs
Coefficient of determination	r^2
Common mode rejection ratio	CMRR
Degrees of freedom	DoF
Diagonal band	db
Distal interphalangeal	DIP
Dorsal interossei	DI
Electromyography	EMG
Extensor digitorum communis	EDC
Extensor indicis	EI
First dorsal interosseous	FDI
First lumbrical	LUM
First palmar interosseous	FPI
Flexor digitorum profundus	FDP
Flexor digitorum superficialis	FDS
Force at the terminal slip	fts
Force from the central slip	fcs
Interphalangeal	IP
Maximum voluntary exertions	MVE
Metacarpophalangeal	MCP
Musculoskeletal disorders	MSD
Normalized root mean square deviation	NRMSD

Palmar interossei	PI
Physiological cross-sectional area	PCSA
Proximal interphalangeal	PIP
Radial band	Rb
Sum of squared activation	SSa
Terminal slip	Ts
Ulnar band	Ub

CHAPTER 1

INTRODUCTION

Proper function of the hand is critical to an individual's autonomy and ability to perform activities of daily living. The hand is susceptible to musculoskeletal and neurological impairments including; tendinopathies, arthritis, connective tissue disease, and dysfunction following a brain injury (Green et al., 2011). Proper hand function is also important in the workplace. In 2011, musculoskeletal disorders (MSD) of the hand and arm, accounted for 10.7% of all MSD claims, and caused over twice the average number of days away from work compared to other MSD injuries in the United States (Bureau of Labor Statistics, 2012). To reduce the risk of developing an MSD, and to improve rehabilitation strategies, there is a need to evaluate forces within the hand. Direct measurement of these forces is not feasible, thus the need for biomechanical modelling is obvious.

A number of musculoskeletal models of the hand and finger have been developed (Fok and Chou, 2010; Wu et al., 2008; Vigouroux et al., 2007; Chalfoun et al., 2005; Sancho-Bru et al., 2001; Li et al., 2000; Keir and Wells, 1999; Valero-Cuevas et al., 1998; Harding et al., 1993; An et al., 1979). From these works, critical advances have been made towards understanding force transmission and coordination in the finger. However, due to the versatility of the finger, a limited number of tasks have been assessed (Placet and Quaine, 2012; Vigouroux et al., 2007; Valero-Cuevas et al., 1998; An et al., 1979). The finger is also anatomically complex and there are many methods we can use to estimate tendon loading. This has led to gaps in our ability to provide accurate predictions for the wide range of manual tasks we can perform.

Static optimization methods are commonly used to estimate tendon loading. Minimizing the sum of squared activation has been used to estimate forces in the finger (Sancho-Bru et al.,

2001; Dennerlein et al., 1998; Brook et al., 1995; Chao et al., 1989). This method preferentially recruits the use of muscles with larger moment arms and physiological cross-sectional areas (PCSA) to reduce muscular effort and delay fatigue (Anderson and Pandy, 1999). However, static optimization, or optimization in general, does not effectively predict the simultaneous activation of agonist and antagonist muscles at a joint, also known as co-contraction (Son et al., 2012; Erdemir et al., 2007; Herzog and Binding, 1993; Hughes and Chaffin, 1988). A number of adapted optimization methods have attempted to estimate co-contraction (Jiang and Mirka, 2007; Brown and Potvin, 2005; Forster et al., 2004; Kellis et al., 2003; Cholewicki and McGill, 1994; Herzog and Binding, 1993). These methods have not been used to estimate forces in the finger, even though co-contraction is essential to performing manual tasks (Valero-Cuevas, 2004; Valero-Cuevas et al., 1998; Thomas and Long, 1968). Optimization methods alone are likely unable to provide solutions that match empirically recorded muscle activity (Vigoroux et al., 2007; Jinha et al., 2006; Ait-Haddou et al., 2004; Raikova and Prilutsky, 2001; Challis and Kerwin, 1993). Vigouroux et al. (2007) used a combined EMG-optimization approach to estimate tendon tensions during static fingertip pressing. The combined method was able to provide tendon tensions that respected mechanical equilibrium while being consistent with individual muscle activation patterns (Vigouroux et al., 2007). EMG-constrained optimization is a promising approach to achieve co-contraction and better match recorded muscle activity (Vigouroux et al 2007; Amarantini and Martin, 2004; Gagnon et al, 2001; Cholewicki and McGill, 1994).

Over the past decade, the increasing popularity of open-source musculoskeletal modelling software (i.e. OpenSim 3.1, Simbios, Stanford, CA; Delp et al., 2007) has provided a way to develop a model and solution method and readily distribute it to researchers. The current

model of the hand available through OpenSim lacks anatomical fidelity. The index finger of the model is actuated only by the four extrinsic muscles (Holzbaur et al., 2005). The intrinsic muscles, such as the interossei and lumbricals, are necessary to perform functional tasks (Fok and Chou, 2010; Vigouroux et al., 2007; Chalfoun et al., 2005; Valero-Cuevas et al., 1998; Buchner et al., 1988). As of July 6th 2014, an Upper Extremity model with updated muscle parameters and pathways has become available (Saul et al., 2014). However, this updated model does not include the intrinsic muscles that are necessary for proper finger control. A model of the finger in OpenSim, that accounts for the complex pathways of the extrinsic and intrinsic muscles, combined with using EMG to constrain an optimization method that considers co-contraction, would improve tendon loading estimates. With an improved ability to predict internal forces, we can better understand mechanisms of injury and develop more appropriate rehabilitation strategies.

CHAPTER 2

REVIEW OF LITERATURE

2.1 Anatomy of the hand

The hand is a complex structure. A number of multi-joint muscles transmit force through the hand. Extrinsic muscles originate in the forearm; while intrinsic muscles originate in the hand (Table 2.1). There are four main extrinsic finger muscles (Figure 2.1). Flexor digitorum profundus (FDP) originates at the coronoid process of the ulna and insert into the base of the distal phalanx of digits 2-5. Flexor digitorum superficialis (FDS) originates on the medial epicondyle of humerus and the coronoid process of ulna and inserts into the base of the middle phalanx of digits 2-5. In addition to flexing the metacarpophalangeal (MCP), proximal interphalangeal (PIP), and distal interphalangeal (DIP) joints, these muscles flex the wrist (note: only FDP flexes the DIP joint). Opposing the flexors is extensor digitorum communis (EDC), which originates from the lateral epicondyle of humerus. There is an additional extensor muscle for the index finger, extensor indicis (EI) which originates on the distal posterior surface of the ulna. The extrinsic extensors insert into the extensor mechanism of each finger (a tendinous aponeurosis on the dorsal surface of each finger). These muscles extend each joint of the finger and the wrist as well.

Intrinsic muscles of the hand include the dorsal and palmar interossei, lumbricals, thenar, and hypthenar muscles (note, thenar and hypothenar muscles will not be examined in this thesis) (Figure 2.2). The dorsal and palmar interossei originate on ulnar and radial sides of the metacarpal shafts and cause abduction and adduction of the MCP joint, respectively. The lumbricals are small muscles that have a unique origin on the FDP tendon. Lumbricals and interossei merge into the extensor mechanism and facilitate MCP flexion while maintaining PIP

and DIP extension. Given this simplified description, note that intrinsic muscles have multiple insertions and are highly variable between people (Eladoumikdachi et al., 2002a; 2002b).

Table 2.1 Extrinsic and intrinsic finger muscles (TCL: Transverse carpal ligament.) Origins, insertions, and actions are summarized from Marieb (2003).

Muscle	Origin	Insertion	Action
	Extrinsic muscles		
Flexor digitorum profundus (FDP)	-Coronoid process of ulna -Interosseous membrane	-Distal phalanx of digits 2-5	-Flexes wrist, MCP, PIP and DIP
Flexor digitorum superficialis (FDS)	-Medial epicondyle of humerus -Coronoid process of ulna; shaft of radius	-Middle phalanx of digits 2-5	-Flexes wrist, MCP and PIP
Extensor digitorum communis (EDC)	-Lateral epicondyle of humerus	-Extensor mechanism of digits 2-5	-Extends wrist, MCP, PIP and DIP
Extensor indicis (EI)	-Posterior surface of distal ulna -Interosseous membrane	-Extensor mechanism of digit 2	-Extends wrist, MCP, PIP and DIP, digit 2
Extensor digiti minimi	-Lateral epicondyle of humerus	-Extensor mechanism of digit 5 -Proximal phalanx of digit 5	-Extends wrist, MCP, PIP and DIP, digit 5
	Intrinsic muscles		
Dorsal interossei (DI)	-Ulnar and radial sides of each metacarpal shaft	-Extensor mechanism	-Flexes MCP joint and extends PIP and DIP -Abducts MCP
Palmar interossei (PI)	-Ulnar and radial sides of the metacarpal shaft	-Extensor mechanism	-Flexes MCP joint and extends PIP and DIP -Adducts MCP
Lumbricals (LUM)	-Lateral side of flexor digitorum profundus tendons in palm	-Extensor mechanism	Flexes MCP joint and extends PIP and DIP -Abducts MCP
Abductor digiti minimi	-Pisiform	-Medial side of proximal phalanx	-Abducts little finger at MCP
Flexor digiti minimi brevis	-Hamate -TCL	-Medial side of proximal phalanx, digit 5	-Flexes little finger at MCP
Opponens digiti minimi	-Hamate -TCL	-Medial side of metacarpal, digit 5	-Brings metacarpal of digit 5 toward thumb

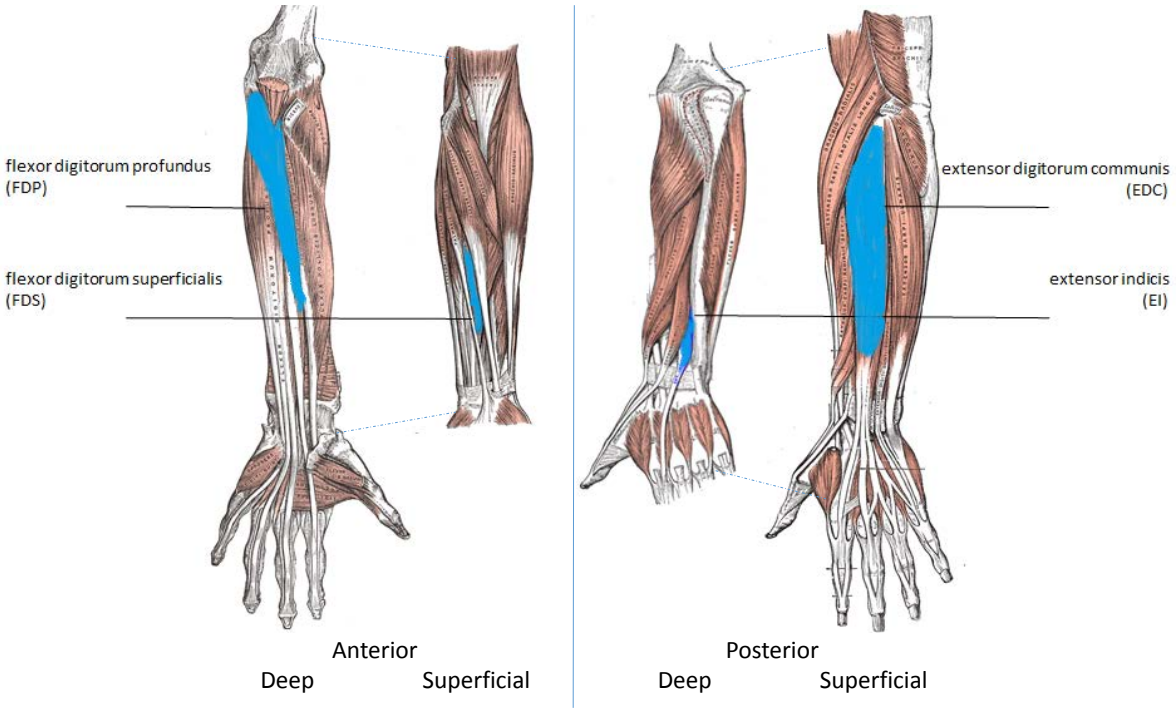

Figure 2.1 Extrinsic muscles of the hand. Left hand view with muscles inserting into the index finger indicated to and shaded over (flexor digitorum profundus (FDP), flexor digitorum superficialis (FDS), extensor digitorum communis (EDC), extensor indicis (EI)) (adapted from, Standing et al., 2008).

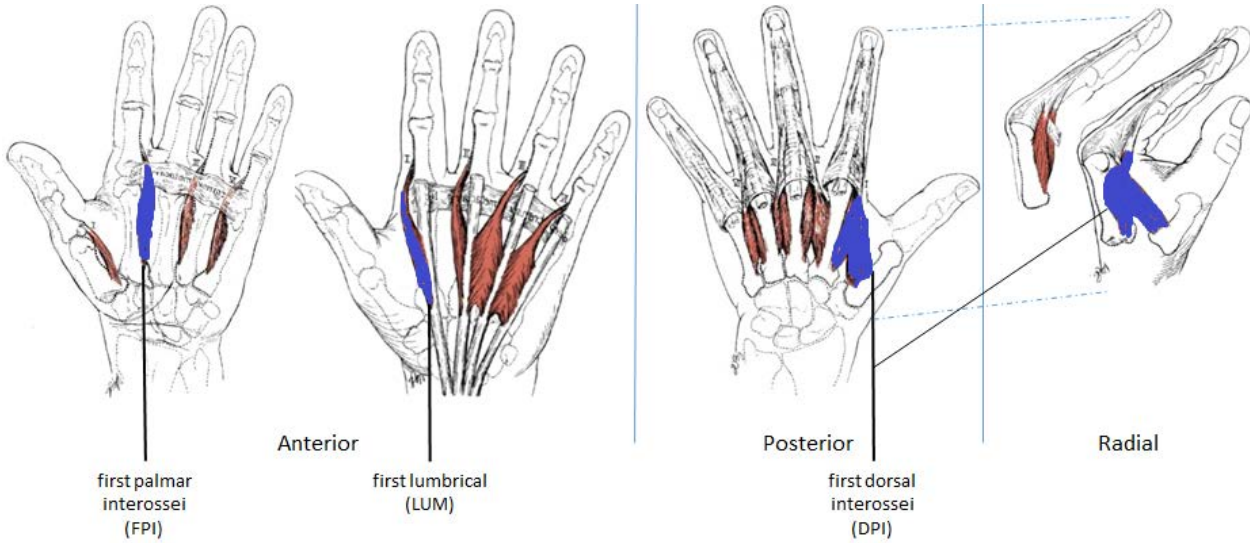

Figure 2.2 Intrinsic hand muscles going to long fingers. Left hand view with muscles inserting into the index finger indicated to and shaded over (first palmar interosseous (FPI), first lumbrical (LUM), first dorsal interosseous (FDI)) (adapted from Palastanga et al., 2011).

In addition to muscles of the hand, there are a number of ligaments and retinacula that influence force transmission. Retinacula are fibrous structures that restrict tendon movement and modify force transmission through the body. The extensor mechanism is an important retinacular structure on the dorsal surface of each finger (Figure 2.3). The extensor mechanism is created by the extrinsic extensors and intrinsic muscle tendons merging into a retinaculum. Since the tendons are woven into this retinaculum, the line of action and the moment arms of each muscle changes depending on finger posture.

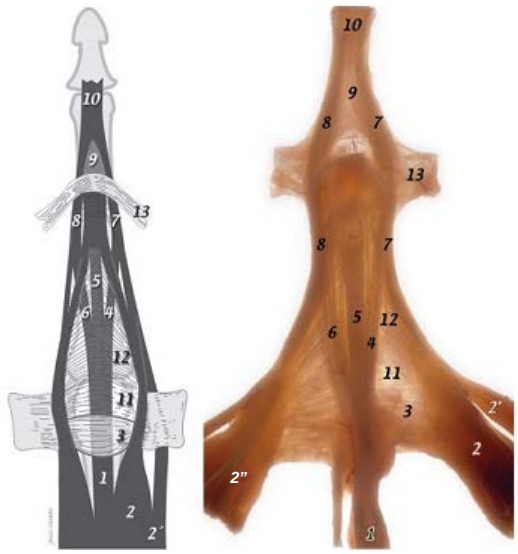

1 **extensor digitorum tendon**
2 **FDI**
2' **LUM**
2'' **FPI**
3 sagittal band
4 **extensor tendon component of radial band**
5 **central slip**
6 **extensor tendon component of ulnar band**
7 **radial band**
8 **ulnar band**
9 triangular ligament
10 **terminal slip**
11 transverse fibers
12 oblique fibers
13 retinacular ligament

Figure 2.3 Dorsal view of the left index finger extensor mechanism. Structures addressed in this thesis are in bold (from Clavero et al., 2003).

In the index finger, five muscles insert into the extensor mechanism (EDC, EI, FDI, FPI, and LUM). Forces from these five muscles are transmitted through the extensor mechanism, and affect the PIP joint via the central slip and the DIP joint via the terminal slip. The central and terminal slips are important components of the extensor mechanism that are commonly used to describe and evaluate force transmission through the finger (Lee et al., 2008; Valero-Cuevas et al., 2008). The extensor mechanism allows the PIP and DIP joints to move independently from

the MCP joint (Beasley, 2003; Harris and Rutledge, 1972; Landsmeer, 1963). The extensor mechanism also provides medial-lateral symmetry of muscle forces. This helps the finger to remain stable while it moves (Zancolli, 1979). All of these structures within the finger have a significant impact on hand function, coordination, and force transmission characteristics (Ranney et al., 1988).

2.2 Force transmission

Interphalangeal coordination has been found to depend on the relationship between intrinsic and extrinsic muscle activity (Chalfoun et al., 2005; Valero-Cuevas et al., 1998; Buchner et al., 1988). Intrinsic muscles have the unique ability to flex the MCP joint while at the same time extend the PIP and DIP joints, and abduct or adduct the finger (Chao and An, 1978). Using a biomechanical model, Fok and Chou (2010) found that high intrinsic muscle activity was needed to maintain mechanical equilibrium during a single static pinch task. Additionally, forces from the lumbrical can alter the force produced by FDP (Ranney et al., 1988). Since the lumbrical originates on the FDP tendon, lumbrical contraction will reduce force in the FDP tendon and help prevent IP joint flexion. To keep the PIP and DIP joints extended, tension from the lumbrical is transferred through the extensor mechanism in conjunction with the extrinsic extensors and interossei on the dorsal aspect of the finger.

How forces are transmitted through the extensor mechanism depends on active and passive muscle forces and finger posture. The tension developed at the central and terminal slips have been found to change with joint angle. Using five index finger cadaver specimens, Lee et al. (2008) applied a constant load to the extrinsic extensor muscles and measured fingertip force at different postures. Through this experiment, they estimated central and terminal slip tension

using a static optimization procedure. Their results indicate a decrease in slip tension with greater joint flexion (Figure 2.4). They also observed a constant ratio of force between the terminal and central slips across postures (1.7:1, terminal slip: central slip ratio). However, the estimate of terminal and central slip forces varies across studies. In a cadaveric study of the middle finger at a single posture, Valero-Cuevas et al. (2007) found the terminal: central slip ratio to range from 1:1.75 to 1:2.25 depending on the tension from each muscle going to the extensor mechanism. There is limited research, with great variability across studies, that estimate central and terminal slip forces. The complex pathways, of the muscles that influence central and terminal slip force, contribute to this difficulty. There is a need to address this deficiency since understanding the relationship between these muscles can provide insight into coordination and control during manual tasks.

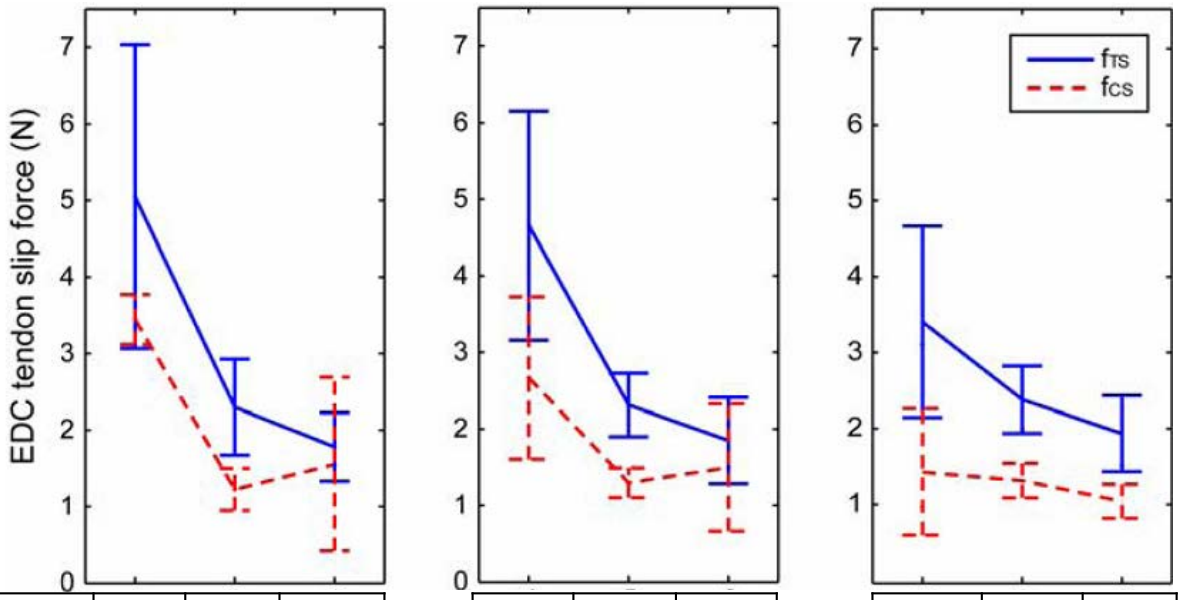

Posture	1	2	3	4	5	6	7	8	9
MCP°	0	0	0	30	30	30	60	60	60
PIP°	0	30	45	0	30	45	0	30	45
DIP°	0	20	30	0	20	30	0	20	30

Figure 2.4 Estimated tension from EDC transferred to the terminal and central slip. Finger flexion increases across the horizontal axis from posture 1 to 9. Slip force on the vertical axis decreases as PIP and DIP joint angles increase within each panel. A consistent terminal: central slip ratio is also observed at each posture. (Force at the terminal slip (f_{TS}) is in the solid line. Force from the central slip (f_{CS}) is in the dotted line). (Adapted from Lee et al., 2008).

2.3 Biomechanical models of the finger

A number of musculoskeletal models have been developed to evaluate forces through the finger (Fok and Chou, 2010; Wu et al., 2008; Vigouroux et al., 2007; Sancho-Bru et al., 2001; Li et al., 2000; Valero-Cuevas et al., 1998; Harding et al., 1993; An et al., 1979). These models are often developed towards assessing a specific task (Placet and Quaine, 2012; Vigouroux et al., 2007; Valero-Cuevas et al., 1998; An et al., 1979). For instance, An et al. (1985) used a biomechanical model to evaluate changes in pinch strength after inhibiting the contribution from different muscles. Similarly, Harding et al. (1993) applied a biomechanical model of the finger to optimize tendon and joint loading during selected piano playing postures with the aim of

reducing overuse injuries. Recently, the versatile nature of the finger has been quantified using modelling techniques as well. Valero-Cuevas et al. (2007) performed simulations where they varied the tension of each muscle going to the finger. The authors concluded that the anatomical complexity of the extensor mechanism allows for the wide variety of forces and movements that we can produce with our finger. However, the nature of the extensor mechanism makes it difficult to model and predict accurate muscle forces. To mitigate this, simplified versions of the extensor mechanism have been used (Valero-Cuevas et al., 2007; An et al., 1985; Zancolli, 1979).

2.3.1 Representing the extensor mechanism with Winslow's Rhombus

Winslow's Rhombus is a simplified version of the extensor mechanism. Originally developed by Winslow (1732) and adapted by Zancolli (1979), this structure is commonly used when modelling the finger (Valero-Cuevas et al., 2007; Kamper et al., 2006; Li et al., 2001; Dennerlein et al., 1998; Harding et al., 1993; An et al., 1985; An et al., 1979). Winslow's Rhombus reduces the complex blanket of connective tissue that makes up the extensor mechanism into a number of bands. Tension from the extrinsic extensors and intrinsic muscles propagate along the finger through these bands. These bands blend together and insert into the central and terminal slips to cause extensor moments at the PIP and DIP joints, while at the MCP joint extension is caused by the extrinsic muscles before merging with the intrinsic muscles (Figure 2.5).

Insertion	Bands	Muscles
Terminal slip (ts)	Radial band (rb)	EDC
		EI
		LUM
		FDI
	Ulnar band (ub)	EDC
		EI
		FPI
Central slip (cs)	Central band (cb)	EDC
		EI
	Diagonal band (db)	LUM
		PI

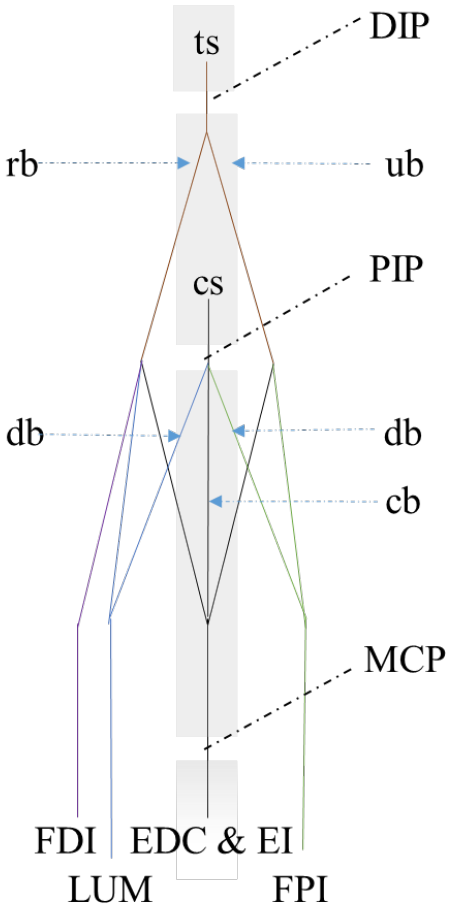

Figure 2.5 Dorsal view of right index finger with Winslow's Rhombus overlaid. Grey rectangles indicate bones of the finger. MCP, PIP, and DIP joints indicated with dotted lines

Often, models using Winslow's Rhombus assume the distribution of tensions through each band is constant (Dennerlein et al., 1998; Harding et al., 1993; An et al., 1985; An et al., 1979). In the model of the hand developed by An et al. (1985), the following relationships were used to estimate muscle forces during isometric pinching tasks:

$$ts \leq rb + ub$$
$$rb \leq {}^{2}/_{3}\,LUM + {}^{1}/_{6}\,EDC + {}^{1}/_{6}\,EI$$
$$ub \leq {}^{1}/_{3}\,FPI + {}^{1}/_{6}\,EDC + {}^{1}/_{6}\,EI$$
$$cs \leq {}^{1}/_{3}\,LUM + {}^{1}/_{3}\,FPI + {}^{1}/_{3}\,FDI + {}^{1}/_{6}\,EDC + {}^{1}/_{6}\,EI \quad (1)$$

where, *ts* and *cs* are the tensions in the terminal and central slips, *rb* and *ub* are tensions in the radial and ulnar bands. These relationships have been able to estimate fingertip forces well for static postures, considering they were assumed by identifying tendon locations from only ten cadaveric specimens (An et al., 1985; An et al., 1979).

In contrast to the assumed distribution of force developed by An et al. (1985), Valero-Cuevas et al. (1998) suggested a force distribution based on the angle of each band with respect to the tendon from which it originates. Angles between bands were adjusted such that the forces exerted through the extensor mechanism best correlated to experimental muscle activities and caused the desired external load. In this method, 62.5% of the force from the extrinsic musculature (EI and EDC) went to the central slip, and the remaining 37.5% was divided evenly between each lateral band. This opposes An et al. (1985) where 16.7% of the force from the extrinsic extensors went to the central slip and an additional 16.7% went to each of the bands. In addition to adjusting the angles of each band for the single posture tested, a number of other

model parameters were adjusted including muscle moment arm and PCSA (Valero-Cuevas et al., 1998).

Kamper et al. (2006) constructed a model of the index finger that incorporated the extensor mechanism using the musculoskeletal modelling software SIMM (Motion Analysis Corporation, Santa Rosa, CA, USA). In this model, LUM and PI muscles insert into the central band with EDC proximal to the PIP joint. However, the lateral bands were not included (Kamper et al., 2006). Given the structure of their model, they were unable to determine the role of the intrinsic muscles at the DIP joint. As such, their results are limited when evaluating the muscle contributions to the production of fingertip forces.

Force distribution patterns through the extensor mechanism are often specific to the model and the task assessed. There is a need to determine force transmission characteristics for a variety of tasks. Moreover, force distribution estimates are subject to how forces are calculated. Static optimization and electromyography (EMG) assisted optimizations are commonly used methods to identify a feasible force distribution for a model. The criteria used in an optimization will have a significant impact on the resulting force distribution, and on how we understand the control of the finger.

2.4 Muscle force prediction methods

2.4.1 Static optimization

Static optimization is commonly used to solve for the muscular load sharing problem (Erdemir et al., 2007). Optimization provides a set of muscle forces while maximizing or minimizing certain factors. These factors are used to create equations known as objective functions, and the objective functions are constrained to only provide solutions that maintain

mechanical equilibrium of the system. Other elements may also be used to constrain the system such as the maximum isometric force of each muscle. While objective functions are created with the intent of providing realistic muscle force estimates, they often produce non-physiological results (Erdemir et al., 2007). There is a need to further develop optimization methods, particularly for estimating hand and finger forces.

The objective function, for the static optimization method used in OpenSim, solves for a set of muscle forces by minimizing the sum of activation squared of all muscles as seen in Equation 2.

$$J = \sum_{m=1}^{N} (a_m)^p \tag{2}$$

where, J is the objective function, N is the number of muscles in the model, a_m is the activation of muscle *m* at a discrete time point, and *p* is the activation exponent (usually squared). Minimizing the sum of squared activation relies on the assumption that a task will be completed by utilizing muscles with advantageous moment arms and large PCSAs to reduce muscular effort and delay fatigue (Anderson and Pandy, 1999). Using these minimized muscle activations, external joint torque is matched through Equation 3 (Zajac, 1988).

$$\tau_j = \sum_{m=1}^{N} [a_m f(F_m^0, l_m, v_m)] r_{m,j} \tag{3}$$

where, τ_j is the moment acting at the j^{th} joint (calculated from the motion of the rigid bodies), *n* is the number of muscles in the model, a_m is the activation of muscle *m* at a discrete time point, f is the force of the muscle (which is constrained by: F_m^0, the muscle's maximum isometric force, l_m, the current length of the muscle, and v_m, the shortening velocity at that time point), and $r_{m,j}$ is the moment arm of that muscle about the j^{th} joint (Hicks, 2013; Thelen et al., 2003; Delp, et al., 2000). Force, length, and velocity properties are normalized with a Hill-type muscle model based on maximum isometric forces and optimal fibre lengths (Zajac, 1988).

For the hand, estimating muscle activity based solely on minimizing muscular effort is likely inappropriate. Simultaneous agonist and antagonist activation is necessary during manual tasks (Nikanjam et al., 2007; Dennerlein et al., 1998 Darling and Cole, 1990). This co-contraction increases the muscular effort above what is required to match a net external joint torque (de Monsabert et al., 2012; Sanei and Keir, 2011). Co-contraction is also required to coordinate finger posture. For example, high intrinsic muscle activity is needed to keep the MCP joint extended during DIP and PIP flexion (Fok and Chou, 2010; Qiu et al., 2009; Valero-Cuevas et al., 1998). This is also true for free flexion movements, in which the extensor muscles act as a brake to control finger movement (Vignais and Marin, 2014; Sancho-Bru et al., 2001; Valero-Cuevas et al., 1998). Although the sum of squared activation objective function (Equation 2) has been widely used, it does not effectively evaluate muscle co-contraction (Son et al., 2012; Erdemir et al., 2007; Herzog and Binding, 1993; Hughes and Chaffin, 1988). Other methods have been developed to help predict co-contraction in static optimization (Jiang and Mirka, 2007; Brown and Potvin, 2005; Forster et al., 2004; Kellis et al., 2003; Cholewicki and McGill, 1994; Herzog and Binding, 1993). Two of these methods are described below since they are used in this thesis. Forster et al. (2004) were able to predict co-contraction by incorporating a 'shift

parameter' into the standard objective function (Equation 4). The shift parameter is a value applied to the activity of each muscle to decrease its contribution to the objective function.

$$J = \sum_{m=1}^{N} (a_m - a_s)^p \quad (4)$$

where, J is the objective function, N is the number of muscles in the model, a_m is the activation of muscle *m* at a discrete time point, *p* is the activation exponent (squared), and a_s is the shift parameter that changes each muscles contribution to the objective function. Forster et al. (2004) demonstrated this method using a single joint model with five muscles. Force-length and force-velocity properties were not included in the calculations. They stated that shift parameters might vary by muscle and task; however, they did not indicate an appropriate range of values (Forster et al., 2004). Finally, there is no physiological basis for introducing a shift parameter to the objective function (Parsa et al., 2013). The applicability of this objective function to the finger still remains to be seen.

Jiang and Mirka (2007) developed an objective function to predict co-contraction with a formula based on a theory from the field of neurophysiology. This objective function is used to represent the hypothesis that there is a weighted combination of reciprocal and coactivation commands controlling agonist and antagonist motorneurons (Feldman 1993, Feldman et al., 1990). The theory suggests that reciprocal commands produce movement while coactivation commands increase joint stiffness and allow for more precise control, but do not contribute to the movement itself (Feldman, 1993; Humphrey & Reed, 1983; Hultborn et al., 1979). A number of studies identify neural systems to support coactivation, either through activation of antagonist

muscles directly (Nielsen and Kagamihara, 1993; Lacquaniti, 1992; DeLuca et al., 1987; Humphrey and Reed, 1983) or through the reduced suppression of antagonist activity by the decrease in Ia inhibitory interneuron activity from agonist muscles (Lewis et al., 2010; Hultborn et al. 1979: Jankowska et al. 1976). The objective function developed by Jiang and Mirka (2007) is the weighted sum of two terms: the first being the standard sum of squared activation (as seen in Equation 2), and a second term being what the authors refer to as the "co-contraction entropy term". The complete objective function from Jiang and Mirka (2007) can be seen in Equation 5.

$$J = (1-W)\sum_{m=1}^{N}(a_m)^p + W\sum_{m=1}^{N} a_m \log a_m \quad (5)$$

where, J is the objective function, N is the number of muscles in the model, a_m is the activation of muscle *m* at a discrete time point, *p* is the activation exponent (squared), and W is the co-contraction weight factor.

The co-contraction entropy term decreases when activities from different muscles are more similar, thus promoting co-contraction. Jiang and Mirka (2007) tested this objective using an elbow flexion task comparing correlation coefficients between muscle forces determined experimentally and from the entropy-assisted optimization. They found a coefficient of determination (r^2) = 0.55 for the triceps during the elbow flexion tasks. The hand load, elbow joint angle, and elbow joint velocity were used in regression equations to estimate the appropriate weight factor for each condition. These equations were task specific and based on one subject's data. Large data sets would need to be collected to use this method for the whole body. Entropy-assisted optimization is a physiologically based approach that merits further

investigation. While it is beneficial to develop optimization parameters to guide a models prediction towards experimental loading conditions, in some cases muscle activities can be used to guide the solution.

2.4.2 EMG-assisted muscle force prediction

Optimization, in conjunction with EMG, has been used under static and dynamic conditions to obtain physiologically realistic estimates of muscle forces (Amarantini and Martin, 2010; Vigouroux et al., 2007; Gagnon et al, 2001; Cholewicki and McGill, 1994). Amarantini and Martin (2010) used a two-step approach to estimate muscle contributions to knee moments during dynamic squatting. The first step required an estimate of the net joint moment along with the agonist and antagonist moments at the knee given the segment kinematics, ground reaction forces, and EMG. In the second step, muscle forces were predicted with static optimization while constraining the solution such that agonist and antagonist moments at the knee were equal to the estimates from the first step. Using this method, they found higher force estimates and a better fit to the experimentally recorded EMG compared to the optimization only approach, especially for the antagonist muscles. While this method shows promise for a single joint model, in the finger muscles often act as agonists at one joint and antagonists at another simultaneously. The complex multi-articular pathways of muscles actuating the finger make it difficult to treat them solely as agonists or antagonists for a task.

EMG assisted optimization has been used to improve finger force predictions. Vigouroux et al. (2007) directly incorporated EMG values into static optimization to estimate tendon tensions during fingertip pressing. They compared results between optimization-only, EMG-only, and a combined EMG optimization method. The combined method provided tendon

tensions that respected mechanical equilibrium, while being consistent with individual muscle activation patterns, for both agonist and antagonist muscles (Vigouroux et al., 2007). The only way to truly validate tendon tension estimates would be through simultaneous *in vivo* measurements, but this is technically impossible given the current technology. However, incorporating muscle activity into optimization constraints may help to provide estimates of muscle forces that more appropriately incorporate antagonist activation.

2.5 Summary

Intrinsic and extrinsic muscles allow us to perform highly specific and powerful tasks with our fingers. These muscles actuate the finger through a connective tissue network called the extensor mechanism. The extensor mechanism is a critically important structure to consider when estimating muscle forces in the finger. To estimate internal forces of the finger, biomechanical modelling often represents the extensor mechanism using a form of Winslow's Rhombus which reduces it into discrete bands to approximate the transfer of force from each muscle to the finger. Each muscle exerts a moment about the finger through the central and terminal slips. Understanding the relationship between the central and terminal slips provides insight to estimating the force each muscle contributes during a task. In addition to the geometry of the model, the calculation method employed is instrumental to predicting accurate muscle forces. Static optimization methods are often used in biomechanical models, but by itself this method often provides non-physiological results. EMG has been used in conjunction with static optimization to improve muscle force estimates. EMG assisted static optimization has the potential to improve muscle force estimates such that mechanical equilibrium of the system can be maintained while accounting for additional muscle activity that is required to perform a

coordinated manual tasks. A biomechanical model and solution method that can provide appropriate muscle force estimates would be useful towards improving surgical and rehabilitation strategies for individuals who have impaired hand function.

2.6 Purpose

The purpose of this thesis was to:

1) Improve the musculoskeletal model of the index finger available through OpenSim by adding intrinsic muscles, incorporating a representation of the extensor mechanism, and adjusting the solution method.
2) Determine how forces are transferred through the finger by assessing central and terminal slip tension ratios, and characterize how these ratios change with force, posture, and movement.
3) Experimentally collect muscle activity during manual tasks to:
    a) Compare with model predicted muscle activities, and
    b) Improve model predicted muscle activities.

2.7 Hypotheses

1) Adding intrinsic muscles, the extensor mechanism, and adjusting the solution method will improve the fit and reduce the difference between predicted and experimental muscle activities.
2) Terminal and central slip tension ratios will be unique to force, posture, and movement. Force will have a greater effect than posture or speed on slip tension ratio.
3) Using experimental muscle activity to drive the prediction of model activity will further improve the fit and reduce the difference between predicted and experimental activities.

CHAPTER 3

METHODS

3.1 Model and solution method development

3.1.1 Model development

The index finger from the OpenSim Upper Extremity model (Holzbaur et al., 2005) has previously been adapted to match *in vitro* experimental data (Kociolek and Keir, 2011). The four extrinsic muscles of the index finger were included in this model. This will be referred to as the Extrinsic-only model and will be used as the basis of development for this thesis. In the current study, all extrinsic and intrinsic muscles controlling the index finger were added (Figure 3.1). Torus and elliptical wrap objects, along with control point functions were used to maintain appropriate moment arms over the complete range of motion for each of the four degrees of freedom in the finger. The first lumbrical (LUM), first dorsal interosseous (FDI), first palmar interosseous (FPI) were added using SIMM to create the Intrinsic model of the index finger (SIMM, Motion Analysis Corporation, Santa Rosa, CA, USA). Maximum isometric force, optimal fibre length, tendon slack length, and pennation angle are used to determine the force generating capacity in the model (Table 3.1) (Delp et al., 2007; Holzbaur et al., 2005). These properties were determined from cadaveric literature (Lieber et al., 1992; Jacobson et al., 1992). Maximum isometric forces were determined using a muscle stress of 45 N/cm^2 multiplied by each muscle's PCSA (Holzbaur et al., 2005). As tendon slack length has not been directly measured, values were adjusted such that the normalized fibre length of each muscle stayed between 0.75-1.25 times the muscles' optimal fibre length throughout the range of motion of each joint (Holzbaur et al., 2005). Muscle properties were normalized and forces were estimated using a Hill-type muscle model (Millard et al., 2013; Zajac, 1988). Ligamentous and passive

forces are not included in the analysis. To account for the extensor mechanism, a novel adaptation of Winslow's Rhombus was developed. In this adaptation, muscles were represented with multiple components and each component was identified by the band or insertion that it connects with (Table 3.1).

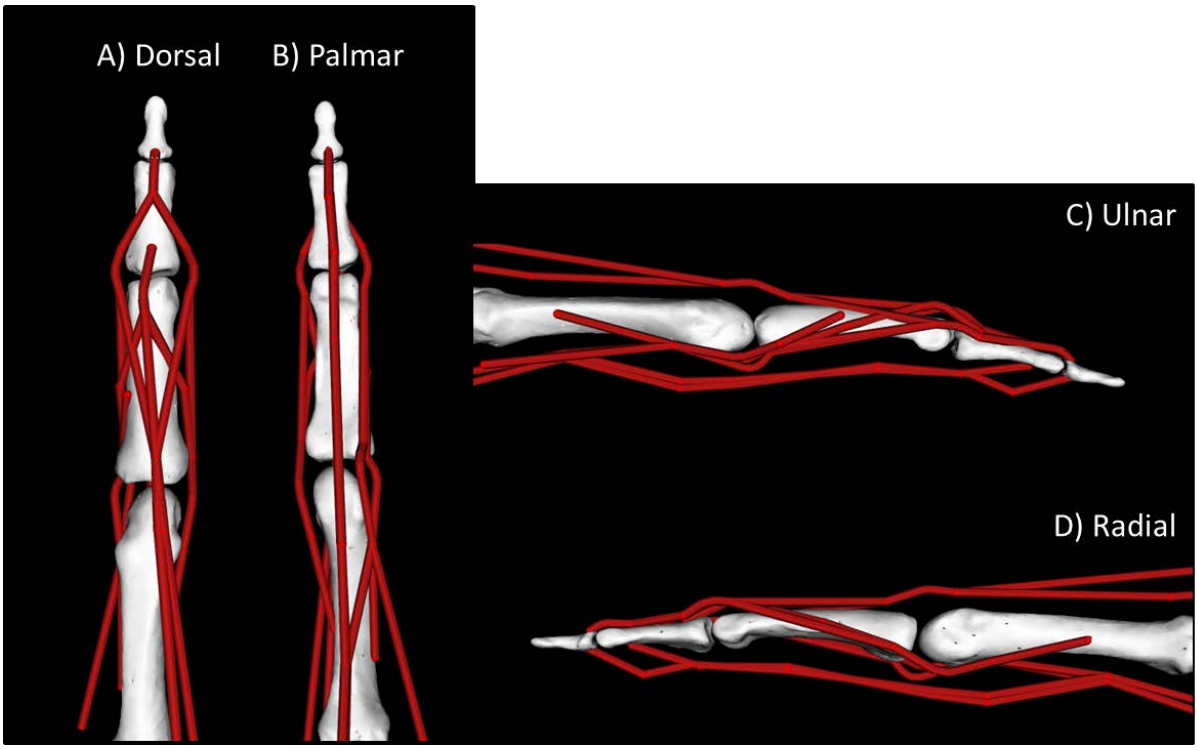

Figure 3.1 Four views of the Intrinsic model A) dorsal, B) palmar, C) ulnar, and D) radial. Muscle paths developed in SIMM (Motion Analysis Corporation, Santa Rosa, CA, USA).

Table 3.1 Intrinsic model muscle parameters. Muscles divided into components are identified by the bands or insertions they connect with from Winslow's Rhombus (Holzbaur et al., 2005; Lieber et al., 1992; Jacobson et al., 1992).

Muscle	Abv.	PCSA (cm^2)	Maximum isometric force (N)	Optimal fibre length (cm)	Tendon slack length (cm)	Pennation (°)
Flexor digitorum superficialis	FDS	1.40	61.24	9.38	30.70	6.00
Flexor digitorum profundus	FDP	1.50	68.27	8.38	32.58	7.00
Extensor digitorum communis	EDC	0.40	18.28	7.86	37.13	3.00
Central slip	EDC_C		12.18	7.88	35.64	3.00
Ulnar band	EDC_U		3.05	7.85	37.88	3.00
Radial band	EDC_R		3.05	7.85	37.88	3.00
Extensor indicis	EI	0.50	21.69	6.51	19.41	6.00
Central slip	EI_C		7.23	6.54	17.95	6.00
Ulnar band	EI_U		7.23	6.5	20.15	6.00
Radial band	EI_R		7.23	6.49	20.12	6.00
First dorsal interosseous	FDI	1.50	67.50	4.10	5.83	9.20
Proximal insertion	FDI_P		54.00	4.10	2.68	9.20
Terminal slip	FDI_T		13.50	4.10	8.97	9.20
First palmar interosseous	FPI	0.75	33.76	3.16	6.53	7.40
Central slip	FPI_C		22.45	3.15	5.55	7.40
Terminal slip	FPI_T		11.31	3.17	7.51	7.40
First Lumbrical	LUM	0.11	4.96	7.07	4.12	1.20
Central slip	LUM_C		1.81	7.07	3.15	1.20
Terminal slip	LUM_T		3.15	7.07	5.08	1.20

3.1.2 Optimization solution methods development

The default static optimization analysis tool available in OpenSim uses the Sum of squared activation objective function (Equation 2). For this thesis, the OpenSim static optimization analysis tool was expanded in two ways. First, two alternative objective functions were added. One being the Shift parameter objective function developed by Forster et al. (2004) (Equation 4), and the other being the Entropy-assisted objective function developed by Jiang and Mirka (2007) (Equation 5). These two solutions aimed to improve the prediction of antagonist activity. In total three objective functions were made available for use during static optimization in OpenSim as seen below:

1) Sum of squared activation (SSa) $$J= \sum_{m=1}^{N} (a_m)^p \quad (2)$$

2) Shift parameter $$J= \sum_{m=1}^{N} (a_m - a_s)^p \quad (4)$$

3) Entropy-assisted $$J= (1-W) \sum_{m=1}^{N} (a_m)^p + W \sum_{m=1}^{N} a_m \log a_m \quad (5)$$

where, J is the objective function, N is the number of muscles in the model, a_m is the activation of muscle *m* at a discrete time point, *p* is the activation exponent (2 in the current study), a_s is the shift parameter that adjusts each muscles contribution to the objective function (0.2 in the current study), and W is the co-contraction weight factor between the two terms (0.5 in the current study). The second expansion to the static optimization analysis tool in OpenSim was that normalized recorded EMG was used to set the constraints for the activity of each muscle

(i.e. EMG-constrained static optimization). In total, three objective functions were used to solve for the muscle load sharing problem, and each solution was either unconstrained or constrained using normalized recorded EMG, then these solution methods were applied to both the Intrinsic and Extrinsic-only models. This gave 12 possible model-solution method combinations for any one task. All changes were incorporated programmatically into OpenSim through a custom analysis tool plugin.

3.2 Experimental Protocol

3.2.1 Participants

Ten (five female, five male) right-hand dominant volunteers aged 25.3 ± 3.1 participated. Exclusion criteria included peripheral nerve disease, tendinopathy, and pain tingling or numbness of the hand. All participants gave informed written consent prior to data collection. The study methods were approved by the university's research ethics board.

3.2.2 Experimental procedure

Participants performed a series of static finger pressing tasks, dynamic unloaded motions, and functional pinching and grasping tasks with the right index finger. Each task was performed twice, once with the elbow supported and once without support. All tasks were block randomized and performed with forearm pronated and the elbow at 90°. During static pressing tasks, participants pressed into the force sensor from their distal phalanx. Forces were applied in four directions, one from each side of their distal phalanx (palmar, radial, dorsal, and ulnar). For every direction force was applied at three levels: 5, 15, and 30 N (Table 3.2, Figure 3.2). For each pressing direction and force level, participants performed two postures, one with their finger flexed and one extended. It is important to note that for the palmar pressing direction

there were two flexed postures in addition to the extended posture. In the first flexed posture ($flexed_a$) both the DIP and PIP joints are flexed, while in the second ($flexed_b$) the DIP remained extended. In total, participants performed 54 static pressing tasks.

Table 3.2 Static pressing tasks participants completed during data collection.

Task	Direction of pressing force
Palmar $Flexed_a$ Palmar $Flexed_b$ Palmar Extended	Pressing down from the palmar side of the distal phalanx, perpendicular to the surface of the force cube
Dorsal Flexed Dorsal Extended	Pressing sideways from the dorsal side of the distal phalanx (forearm semi-prone), perpendicular to the surface of the force cube
Radial Flexed Radial Extended	Pressing sideways from the radial side of the distal phalanx, perpendicular to the surface of the force cube
Ulnar Flexed Ulnar Extended	Pressing sideways from the ulnar side of the distal phalanx, perpendicular to the surface of the force cube

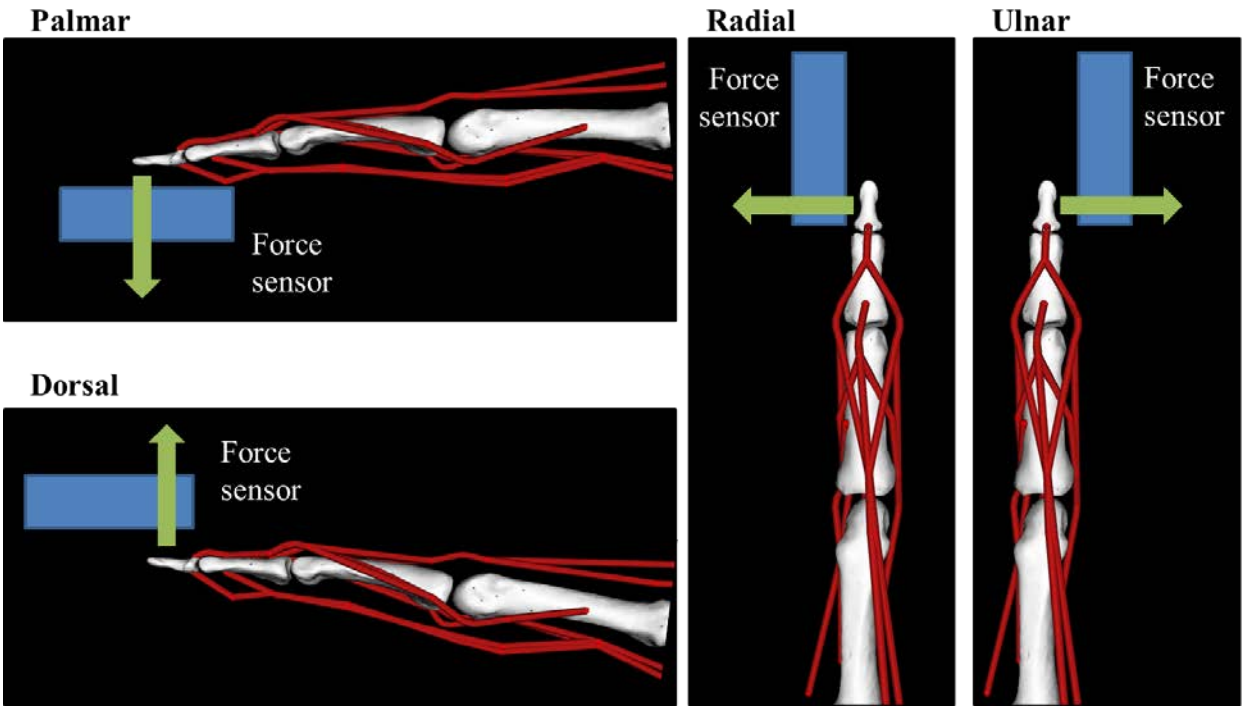

Figure 3.2 Four directions the force was applied in during static pressing tasks. Rectangles identify the forces sensor, and the arrow indicates the direction of force. The diagram shows forces applied in the extended finger posture only, but forces were also applied in the same directions with a flexed posture. Each direction/posture combination was performed at three force levels (5 N, 15 N, and 30 N). Note: palmar pressing direction had additional posture ($flexed_b$) where the DIP remained extended.

Five dynamic unloaded motions were performed at two speeds. Tasks were performed at a fast speed (1.5 repetitions per second) and a slow speed (0.5 repetitions per second). The first three tasks (triggering, tapping, and pointing) required participants to flex and extend each joint of their finger in isolation or in coordination. The last two tasks (circling and ab-adducting) required participants to move the tip of their finger in a circle or in a horizontal line back and forth (Table 3.3, Figure 3.3). Each trial consisted of three repetitions of one task. In total, participants performed 20 dynamic unloaded motions.

Table 3.3 Dynamic tasks participants completed during data collection.

Task	Description of motion
Triggering	Flexing-extending all three phalangeal joints concurrently through the full range of motion of each joint
Tapping	Flexing-extending through the full range of motion of the MCP while keeping the IP joints extended
Pointing	Flexing at the MCP joint while extending the IP joints through the full range of motion of each joint
Circling	Tracing a circle with the fingertip, articulating through the full range of motion of the MCP, keeping the IP joints extended
Ab-adducting	Moving the fingertip medial to lateral, articulating through the full ab-adduction range of motion of the MCP joint, keeping the IP joints extended

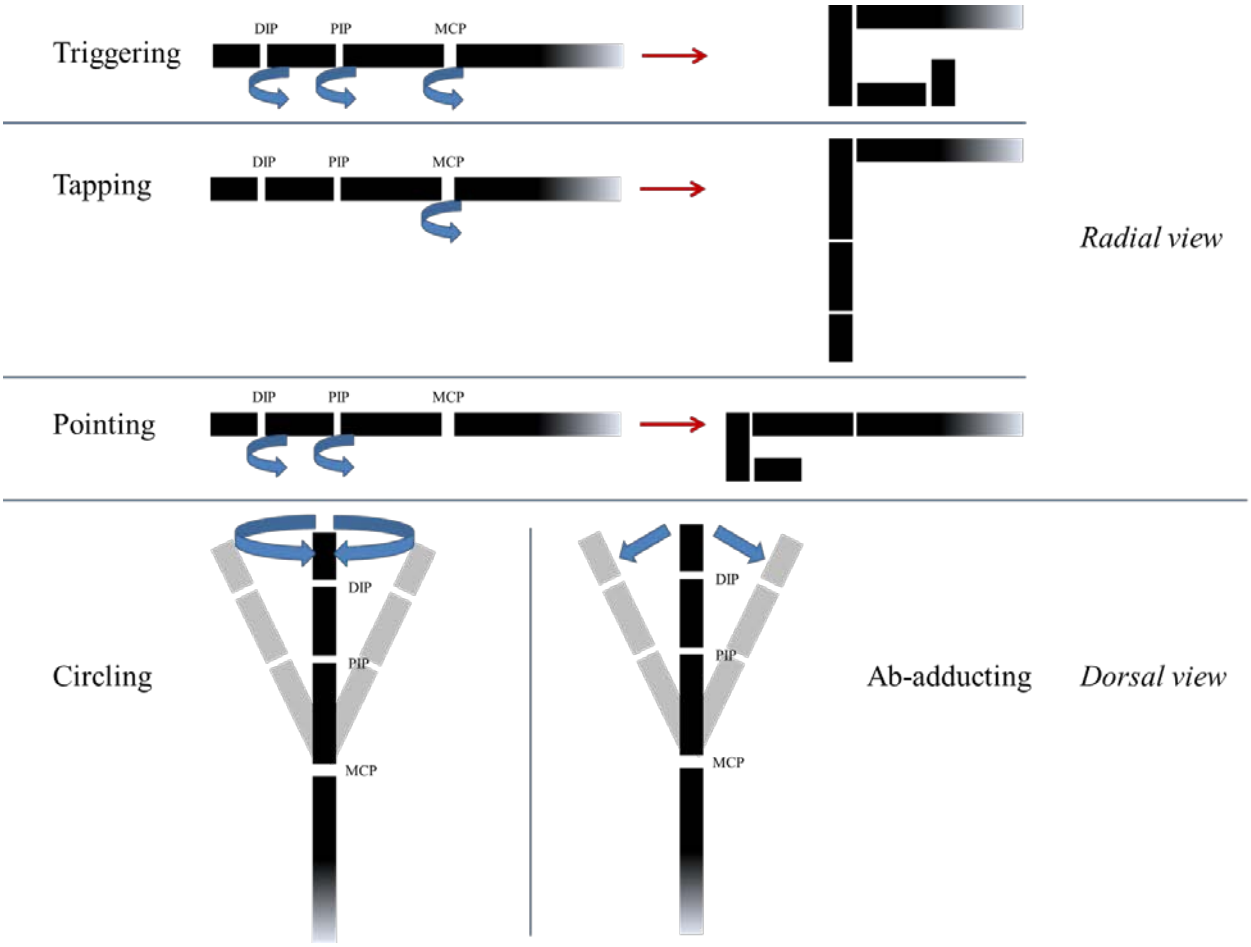

Figure 3.3 Five dynamic unloaded motions. Arrows indicate direction of rotation. Top three images are a radial view of the right index finger showing triggering, tapping, and pointing motions, and the bottom two images are a dorsal view of the circling and ab-adducting motions. Grey shadows indicate how the finger moves while circling and ab-adducting.

Additionally, four functional tasks were assessed (Table 3.4, Figure 3.4). Two pinching tasks and two cap twisting tasks were performed. In one pinch task, participants pressed from the palmar surface of their distal phalanx (pulp pinch). In the other pinch task, participants pressed from the radial side of their distal phalanx (key pinch) (An et al., 1985). For both pinching tasks, the thumb and index were 20 mm apart. The cap twisting tasks required the subject to twist off lids of two different sizes (62 mm and 22 mm in diameter). The task started with the lid closed, and then the participant twisted the lid with their right index finger and

thumb until the cap was off the container.

Table 3.4 Functional tasks participants completed during data collection.

Task name	Description of task
Pulp Pinch	Pinching between the pulp of the index and the thumb
Key Pinch	Pinching between the radial side of the distal phalanx of the index and the thumb
Large Cap Twist	Twist off and on a cap (62 mm in diameter)
Small Cap Twist	Twist off and on a cap (22 mm in diameter)

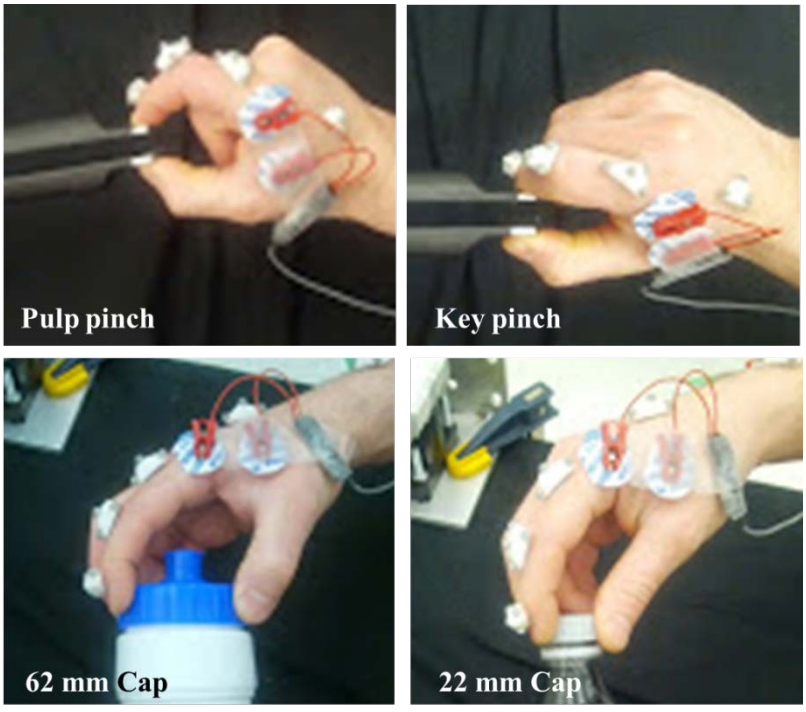

Figure 3.4 Overhead view of the four functional tasks participants performed. Top left: pulp pinch pressing from the palmar surface of the distal phalanx. Top right: key pinch pressing from the radial surface of the distal phalanx. Bottom left: large cap twist and, bottom right: small cap twist.

3.2.3 Data collection

Participants were instrumented with 20 reflective markers (4 mm in diameter) corresponding to 5 marker clusters (4 markers on a rigid base) placed on the dorsal surface of each segment: distal phalanx, middle phalanx, proximal phalanx, metacarpal and the forearm (Figure 3.5). Calibration markers were placed on the dorsal aspect of each joint, and the lateral epicondyle for a single trial. Kinematic data were recorded using a passive optoelectronic motion capture system sampled at 120 Hz (Motion Analysis Corp., Santa Rosa, CA). The static finger pressing tasks were performed against a six-degree of freedom force transducer that was clamped to the table and sampled at 2400 Hz (MC3A-6-100, AMTI, Watertown, MA) (Figure 3.6). Force data were collected and visual feedback was provided using a custom program (LabView 8.5, National Instruments, Texas, USA).

Figure 3.5 Five clusters of reflective markers placed on the dorsal surface of each segment: distal phalanx, middle phalanx, proximal phalanx, metacarpal and forearm.

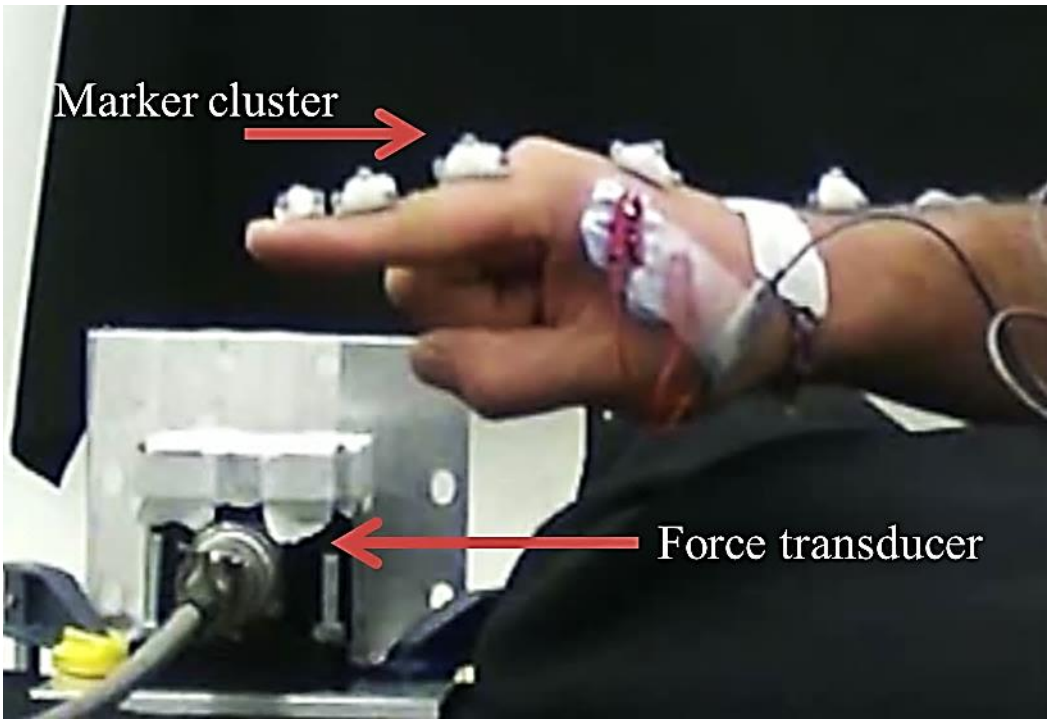

Figure 3.6 Setup of force transducer clamped to the table for a palmar pressing tasks. Participant in an extended finger posture with marker clusters on the dorsal surface of each segment.

During all trials, activity from five muscles (FDS, FDP, EDC, EI, and FDI) was collected using bipolar surface electrodes (Kendall MediTrace 130, Mansfield, MA, USA). Prior to A/D conversion EMG was differentially amplified and band pass filtered between 10 and 1000 Hz (CMRR > 115 dB at 60 Hz, input impedance ~ 10GΩ; AMT-8, Bortec Biomedical Ltd., AB, Canada). EMG was sampled at 2400 Hz (16 bit, USB-6229, National Instruments, TX, USA). All sites were scrubbed with isopropyl alcohol (and shaved where appropriate) prior to applying electrodes. Electrodes were affixed over the belly of each muscle, parallel to fibre direction, and confirmed with palpation and manual resistance tests. Maximum voluntary exertions were performed to determine each muscle's maximal voluntary excitation (MVE). Exertions were held for five seconds and performed three times. Of the two closest trials, the highest peak

activity was used for normalization. Electrode placement and maximal exertion test descriptions can be found in Table 3.5.

Table 3.5 Electrode placement and maximal exertion descriptions (Sanei and Keir, 2013; Leijnse et al., 2008).

Muscle	Electrode placement	Maximal exertion test description
FDS	Distal third of forearm on the lateral border of ulna	Finger in neutral with resistance applied to the palmar side of the middle phalanx
FDP	Distal to the medial epicondyle, proximal and dorsal to the FDS electrode	Finger in neutral with resistance applied to the palmar side of the distal phalanx
EDC	Mid-forearm medial to extensor carpi radialis brevis	Finger in neutral with resistance applied to the dorsal side of the proximal phalanx
EI	Distal end forearm radial to the ulnar head	Finger in neutral with resistance applied to the dorsal side of the proximal phalanx
FDI	Medial side of the second metacarpal	Finger in neutral with resistance applied to the radial side of the middle phalanx

3.2.4 Data analysis

Kinematic data were filtered with a low-pass bi-directional Butterworth filter (f_c = 6 Hz) and imported into OpenSim. Force data were processed with a bi-directional low-pass Butterworth filter (4^{th} order, f_c = 2 Hz). EMG data were smoothed with a bi-directional high-pass Butterworth filter (1^{st} order, f_c = 410 Hz), de-biased, full-wave rectified, then low-pass filtered using a single pass Butterworth filter (4^{th} order, F_c = 2 Hz), and normalized to maximal voluntary exertion (McDonald et al., 2013; Buchannan et al., 2004; Potvin and Brown, 2004). All data were processed using custom program (Matlab 2013b, MathWorks, Inc., Natick, MA).

For each task, 12 unique muscle activity patterns were predicted based on three variables: 1) the model, 2) the activity constraint, and 3) the solution method (Figure 3.7). There were two

models being evaluated in this thesis, either the index finger from the previous Upper Extremity model (referred to here as the Extrinsic-only model) (Kociolek and Keir, 2011; Holzbaur et al., 2005) or the Intrinsic model developed for this study. There were also two activity constraint approaches being evaluated: an optimization-only approach, were activity ranges from 0-100% of MVE, and an EMG-constrained approach where muscle activity can be equal to the normalized recorded EMG value ± 15% of the maximum muscle activity (for example, if normalized EMG = 30%, the predicted muscle activity could be anywhere between 15-45% MVE). Lastly, three objective functions were also evaluated: Sum of squared activation (Delp et al., 2007), Shift parameter (Forster et al., 2004), and Entropy-assisted (Jiang and Mirka, 2007) optimizations.

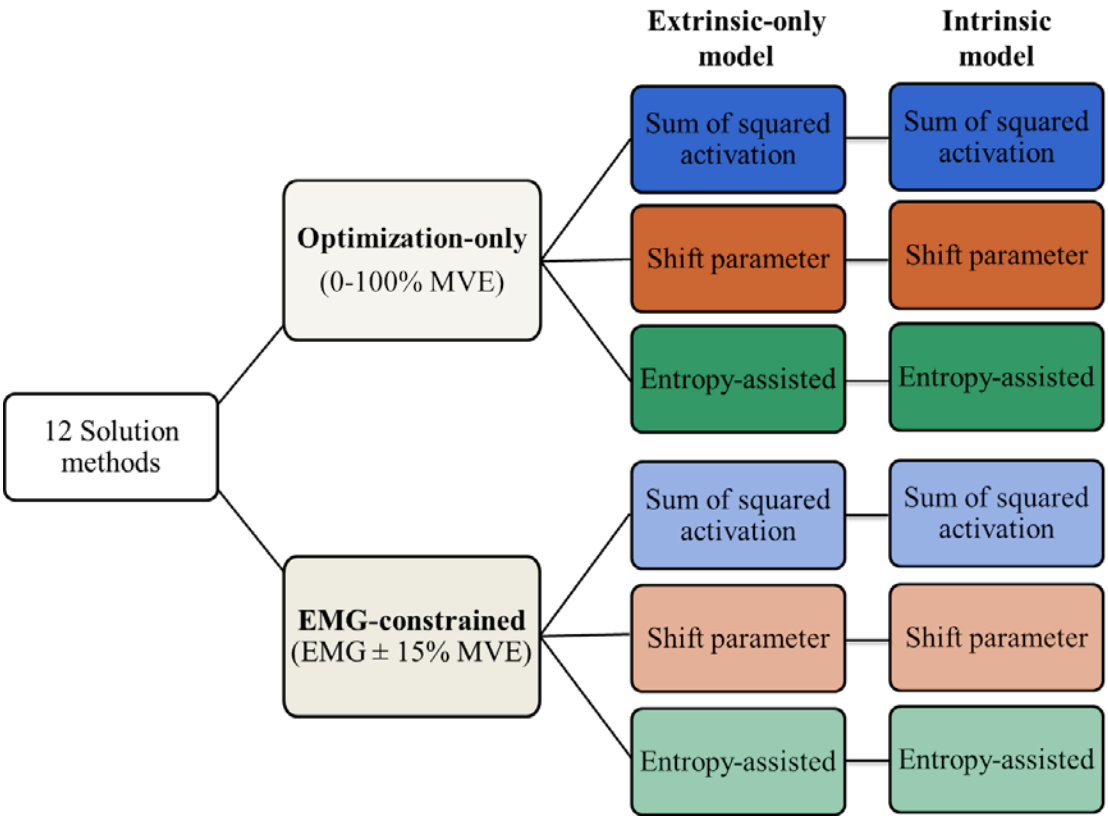

Figure 3.7 Model and solution method combinations resulting in 12 unique muscle force predictions per task. The 12 unique solutions are created from the combination of 2 models x 2 activity constraints x 3 static optimization objective functions.

Two measures of co-contraction were also derived to analyze each model and solution method combination. The two measures were relative antagonist activity and normalized antagonist moments (Equations 6 and 7). These measures were calculated from the average activity of each muscle during the one second static pressing trials. Relative antagonist activity was calculated as the sum of the activity from muscles causing extension divided by the combined activity of muscles causing flexion and extension about a joint. Normalized antagonist moment was the sum of extensor moments from each muscle divided by the net joint moment. Similar calculations have been made to assess the relative contribution of extensor muscles towards total muscle activity and moment (van Dieën et al., 2003; Osu et al., 2002).

$$Relative\ antagonist\ activity = \frac{\sum\ activity\ from\ muscles\ causing\ extension}{\sum activity\ from\ muscles\ causing\ flexion\ and\ extension} \quad (6)$$

$$Normalized\ antagonist\ moment = \frac{\sum moments\ from\ muscles\ causing\ extension}{Net\ joint\ moment} \quad (7)$$

Lastly, force at the terminal and central slip was calculated as the sum of all muscle components inserting into that slip. For static tasks, forces were taken from the average value during the one second trial. For dynamic tasks, the forces were calculated at each instant during the cycle. Terminal and central slip contributions were determined as the force at that slip divided by the total slip force (terminal slip force plus central slip force).

3.2.5 Statistical analysis

Three of nine static pressing tasks were assessed. The three palmar pressing postures (palmar flexed$_{a,}$ palmar flexed$_{b,}$ and palmar extended) were selected since they better align with and may be compared to previous literature (Paclet and Quaine, 2012; Vigouroux et al., 2007; An et al., 1985). Two 3x3x2x6 repeated measures ANOVAs were used to determine differences between the Intrinsic and the Extrinsic-only models' fit with recorded muscle activity. Two dependent variables were used to assess fit in separate calculations: one being the coefficient of determination (r^2) as an index of shape similarity, and the other being normalized root mean square deviation (NRMSD) to reflect differences in magnitude. These ANOVAs were conducted for each of the four extrinsic muscles (FDS, FDP, EDC, EI). For both repeated

measures ANOVAs the independent variables were: posture (3), force (3), model (2), and solution method (6). A similar analysis was conducted with all five dynamic tasks. The same dependent variables, r^2 and NRMSD, were used for each muscle. However for dynamic tasks, 5x2x2x6 repeated measures ANOVAs were performed where the independent variables for were: motion (5), speed (2), model (2), and solution method (6). A summary of the ANOVAs performed for static and dynamic tasks can be found in Table 3.6.

Additionally, for the three static pressing tasks, repeated measures ANOVA's were conducted with the two measures of co-contraction (relative antagonist activity and normalized antagonist moment). These two measures served as dependent variables in separate 4-way, repeated measure ANOVAs, while the independent variables were: posture (3), force (3), model (2), and solution method (6) (Table 3.6). Lastly, to determine changes in terminal slip contribution as a function of posture and force during static pressing tasks a 3x3 repeated measures ANOVA was conducted using forces derived from the EMG-constrained entropy-assisted static optimization solution method. The dependent variable was the terminal slip contribution. The two independent variables were posture (3) and force (3) (Table 3.6).

For all repeated measures ANOVAs, Greenhouse-Geisser corrections were applied where the assumption of sphericity was violated, as assessed by Mauchly's test of sphericity, $p < 0.05$. Bonferroni adjustments were made for multiple comparisons, and post-hoc univariate repeated measures ANOVAs were conducted following significant interaction effects.

In addition to the ANOVAs performed, descriptive statistics were evaluated for terminal and central slip contributions during dynamic tasks. The maximum, minimum, and range of slip contribution during all dynamic tasks were found for fast and slow motions. Mean and standard

deviation of the collected muscle activity for the extrinsic muscles are also presented for each static pressing posture and force.

Table 3.6 Summary of ANOVAs performed for static pressing and dynamic tasks

RM-ANOVA	Independent variables	Dependant variable	Description
4-way	Posture (3) Force (3) Model (2) Solution method (6)	NRMSD between predicted and experimental muscle activity	Performed for each of the 4 extrinsic muscles (FDP, FDS, EDC, EI) on static pressing tasks
4-way	Posture (3) Force (3) Model (2) Solution method (6)	r^2 between predicted and experimental muscle activity	Performed for each of the 4 extrinsic muscles (FDP, FDS, EDC, EI) on static pressing tasks
4-way	Motion (5) Speed (2) Model (2) Solution method (6)	NRMSD between predicted and experimental muscle activity	Performed for each of the 4 extrinsic muscles (FDP, FDS, EDC, EI) on dynamic tasks
4-way	Motion (5) Speed (2) Model (2) Solution method (6)	r^2 between predicted and experimental muscle activity	Performed for each of the 4 extrinsic muscles (FDP, FDS, EDC, EI) on dynamic tasks
4-way	Posture (3) Force (3) Model (2) Solution method (6)	Mean relative antagonist activity (Equation 6)	Calculated as an average value during each static pressing task. Mean of the DIP, PIP, and MCP joints)

Table 3.6 continued

RM-ANOVA	Independent variables	Dependant variable	Description
4-way	Posture (3) Force (3) Model (2) Solution method (6)	normalized antagonist moment (Equation 7)	Calculated as an average value during each static pressing task. Mean of the DIP, PIP, and MCP joints)
2-way	Posture (3) Force (3)	Terminal slip contribution to total slip force	Calculated using the Intrinsic model and the EMG-constrained Entropy assisted objective function for static pressing trials

3.3 Model and solution method parameter rationale

Given the nature of the modelling environment and the musculoskeletal system, a number of decisions needed to be made prior to the complete analysis to obtain the robust results while keeping to the scope of the thesis. Results from the preliminary investigation related to these decisions are discussed in the following sections.

3.3.1 Linear scaling

The model segment lengths were scaled according to participant specific anthropometrics. Muscle properties including: optimal fibre length, tendon slack length, and pennation angle were scaled linearly with the physical dimensions of each participant as well. Maximum isometric force of each muscle was determined using a muscle stress of 45 N/cm^2 multiplied by each muscle's PCSA (Holzbaur et al., 2005; Lieber et al., 1992; Jacobson et al., 1992). Upon initial investigation, both models were unable to generate the forces produced during the experimentally recorded pressing tasks. An initial estimate of the strength needed by the model to generate the necessary force was determined using Equation 8:

$$estimate\ of\ strength\ required\ by\ the\ model = \frac{required\ net\ MCP\ moment\ from\ inverse\ dynamics}{approximate\ net\ MCP\ moment\ experimentally\ produced\ by\ the\ muscles} \quad (8)$$

The approximate net MCP moment produced by the muscles (the denominator of Equation 8) was defined as the sum of the extrinsic muscles maximum isometric force multiplied by each muscles moment arm and normalized activity during the high force palmar pressing tasks. It was found that scaling all the muscles by a factor of three allowed both models to generate the

required forces. Linearly scaling forces to this degree has previously been done to allow a model to function while maintaining the force relationship between muscles (Arnold et al., 2010; Delp et al., 1990).

3.3.2 Optimization settings

In order to use optimization solutions that aimed to increase the prediction of co-contraction, two additional parameters needed to be incorporated. For the Shift parameter objective function (Equation 4) the additional parameter was the shift value, a_s. For the Entropy-assisted objective function (Equation 5) the additional parameter was the weight factor, *W*. To determine the most appropriate values, static optimization was run multiple times with varying parameter values for a subset of data (static palmar pressing in the flexed$_a$ and extended postures at 5 and 30 N for one participant on EDC). The shift value, a_s, and weight factor, *W* parameters were altered from 0-1 in increments of 0.1. At each increment, static optimization was run and normalized root mean square deviations (NRMSD) between predicted and experimental results were evaluated. The parameter values that provided the lowest NRMSD between predicted and experimental activity was used for the complete analysis. The shift parameter selected was 0.2, indicating that every normalized muscle activity would be reduced by 20% MVE when it was applied to the objective function. This is similar to the values used by Forster et al. (2004). The weight factor used for Entropy-assisted optimization was 0.5, in other words an equal balance between terms of the objective function. For both parameters, the authors suggested that the value is likely to be task and model specific. It would be ideal to identify subject and task specific parameters. However, these values were used for all tasks and subjects to demonstrate the overall utility and limitations of the Intrinsic model and static optimization solution methods.

Future work should be directed to specifying these values. Finding the most appropriate shift parameters and weight factors will help maximize the fit and reduce the error between predicted and experimental activity.

3.3.3 Determining maximum isometric forces

The Intrinsic model was designed to have muscle paths that represent the extensor mechanism. As such, all the muscles that insert to the extensor mechanism are divided into either two or three components (EDC, EI, FDI, FPI, LUM). For example, the LUM muscle is comprised of two separate components, one that inserts at the central slip (LUM_C) and one that inserts on the terminal slip (LUM_T). While the two components have similar paths proximally, their paths differ distally. This made it possible to estimate the terminal and central slip tension. Based on the software, there is no way to link different muscle paths or identify that they are part of the same muscle, thus they are effectively treated as unique muscles. To mitigate this limitation, a preliminary analysis was performed to determine how to distribute forces within each multi-component muscle such that the results most closely match experimental activity. In the first step of the analysis, the maximum isometric force of each muscle was divided equally into the number of components that muscle had (either 2 or 3 components). Then, a scale factor was used to adjust the maximum isometric force of each component such that it varied from 20 to 180% (in 20% increments), while the other component(s) made the remainder of that muscle's total maximum isometric force. In doing this, the total muscle force was preserved. A Sum of squared EMG-constrained static optimization was run for each set of component muscle forces, and then activation profiles were compared to experimentally recorded EMG. This analysis was completed for one subject in the $flexed_a$ (where both the DIP and PIP are flexed) and extended

postures at 5 and 30 N force levels. The set of component forces that gave the lowest NRMSD on average across the trials tested in the preliminary analysis was used. The scale factors used to optimize maximum isometric forces for each component can be seen in Table 3.7.

Table 3.7 Scale factor used to adjust maximum isometric forces of each muscle component to optimize muscle force distribution such that it minimized NRMSD with experimental activity. Initial maximum isometric forces were set to the maximum force of the muscle divided by the number of components (either 2 or 3).

Muscle component	Scale Factor
EDC_C	2
EDC_U	0.5
EDC_R	0.5
EI_C	1
EI_U	1
EI_R	1
FDI_P	1.6
FDI_T	0.4
FPI_C	1.33
FPI_T	0.67
LUM_C	0.73
LUM_T	1.27

The trend towards increased force going to the central slip compared to the terminal slip is supported in previous works. Valero-Cuevas et al. (2007) determined tension to range from 1:1.75-2.25 (terminal: central slip). When modelling larger muscle groups, activation levels from muscle components are commonly lumped into one value (Hamner et al., 2010; Arnold et al., 2010). However, to determine a muscle's contribution to central and terminal slip tension in the finger, some variability was needed between compartments. An alternative method would

have been to analyze each task and force level individually, varying the component forces iteratively and finding the closest match to the recorded activity. However, this would require a unique model for each task and force level, which would be at odds with the purpose of this thesis. Additionally the analysis would be prohibitively time consuming (at an average of 4 hours per run with 6 solution methods, and 9 conditions it would take 216 hours (9 days) per subject, for the three static pressing trials alone).

CHAPTER 4

RESULTS

4.1 Experimental results

Overall, participants directed 98.4 ± 1.7% of the resultant force directly down into the force cube. Across the three pressing postures, participants generated a mean force of 4.9 ± 0.4 N for the 5 N tasks, 14.2 ± 0.8 N for the 15 N tasks, and 25.0 ± 3.7 N for the 30 N tasks. Mean vertical force, and the contribution of the vertical force to the resultant, can be seen in Figure 4.1). Mean and standard deviations of muscle activity for static pressing tasks are presented in Table 4.1. Additional information related to mean joint angles and speed of motion can be found in appendix A).

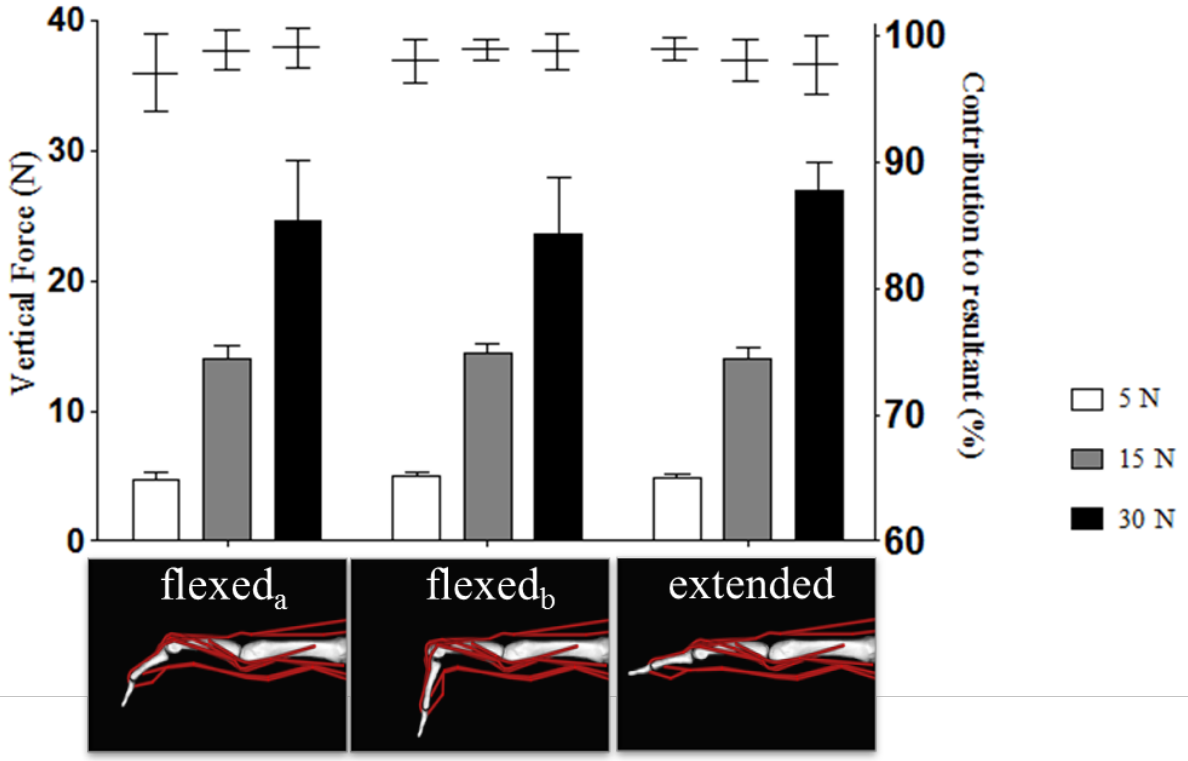

Figure 4.1 Absolute vertical force and vertical force percent contribution to resultant at each static pressing posture and force level. Left axis corresponds to bars at each force and posture. Right axis corresponds to the percent contribution to resultant indicated by the horizontal line above each bar. In flexed$_a$ both the PIP and DIP joint are bent, while in flexed$_b$ the DIP remained extended.

Table 4.1 Normalized activity for the extrinsic muscles (expressed in percent MVE). Average activity during the three palmar pressing tasks at each posture and force are presented.

Posture	Force	FDS	FDP	EDC	EI
flexed$_a$	5 N	11.0 (5.7)	12.1 (5.0)	11.7 (2.7)	13.6 (7.1)
	15 N	24.9 (11.6)	24.1 (9.8)	19.8 (8.1)	20.3 (9.3)
	30 N	38.8 (18.9)	40.6 (12.2)	31.1 (11.5)	33.0 (13.3)
flexed$_b$	5 N	11.5 (4.6)	13.8 (5.7)	10.4 (3.3)	12.2 (6.6)
	15 N	23.3 (9.3)	30.6 (11.9)	17.0 (7.4)	19.1 (9.0)
	30 N	36.2 (10.5)	51.3 (18.1)	23.0 (9.5)	28.8 (15.3)
extended	5 N	12.1 (6.4)	14.3 (5.1)	10.2 (3.6)	10.6 (4.9)
	15 N	21.0 (9.5)	26.4 (8.9)	13.6 (5.8)	15.1 (8.4)
	30 N	39.1 (15.4)	50.0 (14.2)	27.7 (11.8)	30.3 (16.8)

4.2 Modelling results

Based on the volume of data to analyze, only findings which most directly address the purpose of this thesis are included in the following sections. The complete list of significant results from the repeated measures ANOVAs identified in the Statistical analysis section can be found in Appendix A (Table A.3). For the results presented below, many findings were consistent across multiple muscles. In these cases, the relevant muscles have been identified and the statistics presented are from the muscle with the highest significance (i.e. the p value closest to 0.05).

4.2.1 Solution method and muscle activity

During static palmar pressing, EMG-constrained methods provided lower NRMSD than Optimization-only methods for all muscles ($F_{1.036, 9.326} = 6.493$, $p < .030$ for the FDP) (Figure 4.2, Note: degrees of freedom adjusted from Greenhouse-Geisser corrections for sphericity). For FDS and EDC, when activity was constrained by EMG, co-contraction objective functions gave lower NRMSD than the Sum of squared activation (SSa) objective function ($F_{1.544, 13.895} = 28.285$, $p < .046$). Across solution methods, posture did not affect the NRMSD during static pressing ($F_{1.995, 17.915} = 0.981$, $p > .394$). However, there was a main effect of force for the EDC. Pressing at the 30 N force level provided lower NRMSD (11.5 ± 5.2) then pressing at the 5 N force level (23.4 ± 9.3) across solution methods ($F_{1.91, 17.22} = 8.249$, $p > .003$).

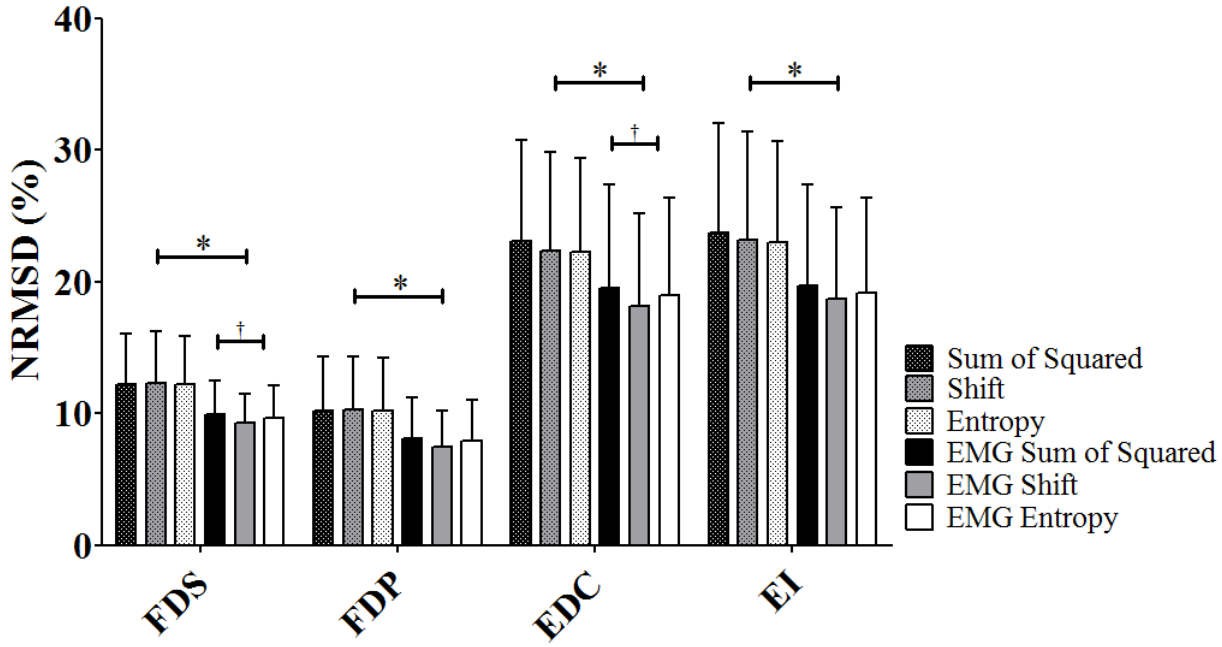

Figure 4.2 Solution method main effect of NRMSD for extrinsic muscles during static pressing.
* Significant difference between EMG-constrained and Optimization-only methods.
† Significant difference between SSa and co-contraction objective functions.

For dynamic trials, the 5x2x2x6 RM ANOVA revealed that motion did not affect the NRMSD for FDS or EDC ($F_{1.714, 15.422} = 2.614$, $p > 0.111$). For FDP and EI, there were differences in NRMSD depending on the motion. For FDP, circling had a higher NRMSD (13.5 ± 6.2) than pointing (7.6 ± 3.2) ($F_{4, 36} = 4.740$, $p < .004$). However for EI, Ab-adducing had a higher NRMSD (5.5 ± 1.8) than circling (3.6 ± 1.7) ($F_{4, 36} = 4.788$, $p < .003$). Overall, the average NRMSD across the five motions was 8.1 ± 1.4%. There was a Speed*Method interaction for FDS and FDP. At slow speeds but not at fast speeds, activity predicted from co-contraction objective functions was closer to the experimental values compared to the SSa objective ($F_{1.05, 9.451} = 14.246$, $p < .037$).

Furthermore, across all dynamic trials, extensor muscle activity predicted from EMG-constrained methods had lower NRMSD than Optimization-only methods ($F_{1.098, 9.88} =$

26.452, $p < .044$) (Figure 4.3). For EDC, co-contraction objective functions gave lower NRMSD than SSa solutions ($F_{1.035, 9.312} = 28.056$, $p< 0.013$). With flexor muscles, there was an interaction between the model and solution method. For FDP, when using the Intrinsic model, EMG-constrained Entropy optimization had lower NRMSD than EMG-constrained SSa optimization ($F_{1.01, 9.094} = 13.064$, $p < .019$). Using the Extrinsic-only model, EMG-constrained co-contraction optimizations had lower NRMSD than all other solution methods ($F_{1.069, 9.625} = 17.762$, $p < .031$).

With EMG-constrained solutions, a decrease in NRMSD was often accompanied by a decrease in the fit between predicted and experimental activity. The EMG-constrained SSa method averaged a higher NRMSD (7.00 ± 2.13) and r^2 (0.38 ± 0.15), while the EMG-constrained co-contraction methods averaged a lower NRMSD (6.62 ± 2.05) and r^2 (0.31 ± 0.13). Coefficients of determination (r^2) for dynamic trials were generally low across solution methods, ranging from 0.07 ± 0.04 in the FDS when using optimization-only methods to 0.62 ± 0.21 for the EI using an EMG-constrained solution method (Table 4.2). Speed also influenced the explained variance (r^2) between predicted and experimental activity. There was a Speed*Method interaction from the repeated measures ANOVA performed for each muscle. At slow speeds, r^2 values were higher for all muscles when using the EMG-constrained SSa solution compared to EMG-constrained co-contraction optimizations ($F_{1.103, 9.931} = 6.062$, $p = 0.031$). At fast speeds, the r^2 for EDC was higher when using the EMG-constrained SSa method compared to the EMG-constrained Entropy method ($F_{1.464, 13.117} = 10.367$, $p = 0.018$).

Between the two co-contraction objective functions, the Entropy-assisted objective gave lower NRMSD than the SSa objective more often than the Shift parameter objective. In five of nine cases the Entropy-assisted objective function gave lower NRMSD than the SSa while the

Shift parameter objective did not. The Entropy-assisted objective was uniquely significant for FDS and EDC during static pressing, FDP and EDCI in dynamic trials, and for EI during fast dynamic trials. However, the Shift parameter objective was uniquely significant in only one condition, for EI during static pressing. Otherwise, both co-contraction methods produced lower NRMSD than the SSa method.

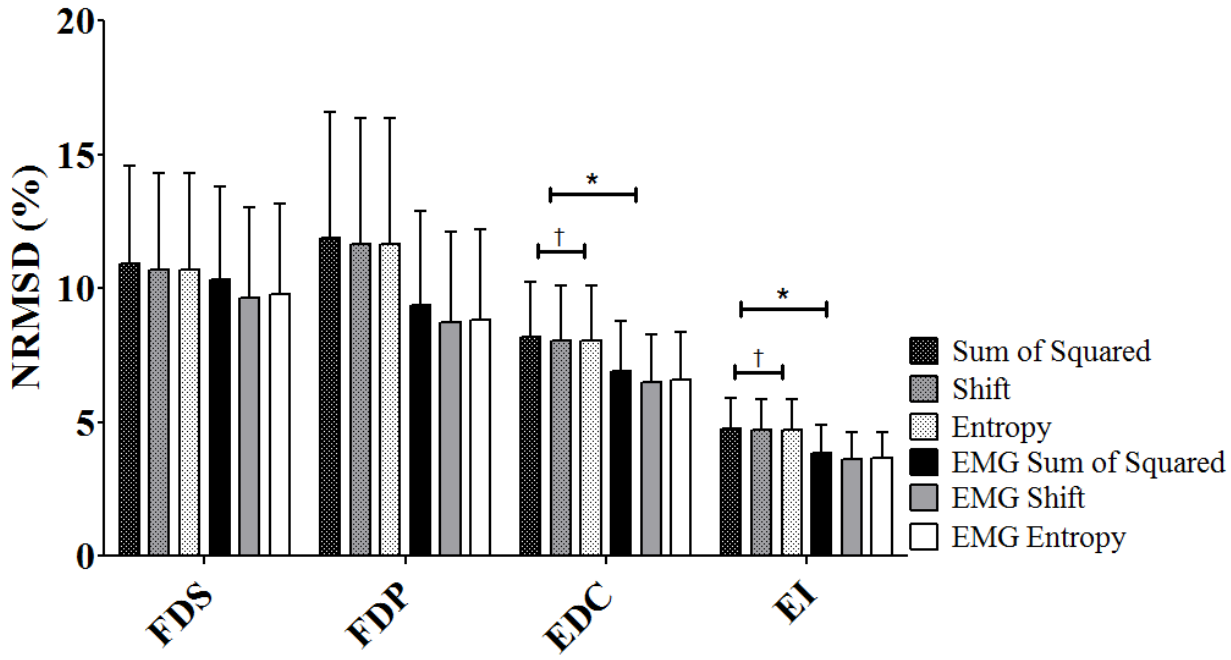

Figure 4.3 Mean NRMSD for extrinsic muscles by solution method during dynamic tasks.
* Significant difference between EMG-constrained and Optimization-only methods.
† Significant difference between SSa and co-contraction objectives.

Table 4.2 Coefficients of determination (r^2) between predicted and experimental activity during dynamic trials for each muscle and solution method at slow and fast speeds.

		EMG-constrained Sum of squared activation	EMG-constrained Shift	EMG-constrained Entropy	Optimization-only Sum of squared activation	Optimization-only Shift	Optimization-only Entropy
FDS	Fast	0.25 (0.10)	0.19 (0.07)	0.21 (0.08)	0.22 (0.07)	0.22 (0.09)	0.21 (0.10)
	Slow†	0.19 (0.10)	0.13 (0.09)	0.11 (0.10)	0.11 (0.06)	0.07 (0.04)	0.07 (0.04)
FDP	Fast	0.32 (0.21)	0.26 (0.19)	0.26 (0.19)	0.24 (0.14)	0.23 (0.09)	0.21 (0.10)
	Slow†	0.32 (0.28)	0.22 (0.17)	0.26 (0.23)	0.11 (0.07)	0.07 (0.05)	0.08 (0.05)
EDC	Fast‡	0.37 (0.18)	0.30 (0.11)	0.31 (0.16)	0.30 (0.07)	0.14 (0.05)	0.13 (0.04)
	Slow†	0.31 (0.15)	0.21 (0.13)	0.26 (0.16)	0.12 (0.05)	0.08 (0.04)	0.08 (0.04)
EI	Fast	0.55 (0.25)	0.45 (0.20)	0.48 (0.23)	0.35 (0.08)	0.18 (0.06)	0.18 (0.05)
	Slow*†	0.62 (0.21)	0.47 (0.20)	0.53 (0.21)	0.12 (0.04)	0.08 (0.03)	0.08 (0.03)

* Significant difference between EMG-constrained and Optimization-only methods.

† Significant difference between EMG-constrained SSa and EMG-constrained co-contraction methods.

‡ Significant difference between EMG-constrained SSa and EMG-constrained Entropy methods.

4.2.2 Model and muscle activity

During static pressing tasks, only for EI were there differences in NRMSD between the Extrinsic-only and the Intrinsic models. There was a Model*Method interaction wherein the Extrinsic-only model provided lower NRMSD (17.1 ± 7.1) than the Intrinsic model (21.2 ± 7.7) when using EMG-constrained co-contraction optimization methods ($F_{1, 9} = 16.504$, $p < .003$). During dynamic tasks, NRMSDs were similar between models as differences were dependent on the solution method.

Across all dynamic tasks, the differences between models were specific to the solution method and muscle. Intrinsic model r^2 values were higher for FDP when using Optimization-only co-contraction solutions methods ($F_{1, 9} = 6.758$, $p < .029$). Similarly, r^2 was higher from the Intrinsic model for EI when using EMG-constrained co-contraction optimization solutions ($F_{1, 9} = 9.534$, $p < .013$). In contrast, for EDC the r^2 values from the Extrinsic-only model were higher when using two of the six solution methods (either the EMG-constrained SSa or EMG-constrained Entropy optimization method ($F_{1, 9} = 8.085$, $p = .019$) (Table 4.3).

Table 4.3 Coefficients of determination (r^2) between predicted and experimental activity during dynamic trials for each muscle and solution method determined by the Intrinsic and the Extrinsic-only models.

Muscle	Model	EMG-constrained Sum of squared activation	EMG-constrained Shift	EMG-constrained Entropy	Optimization-only Sum of squared activation	Optimization-only Shift	Optimization-only Entropy
FDS	Intrinsic	0.21 (0.08)	0.18 (0.08)	0.16 (0.09)	0.17 (0.05)	0.16 (0.08)	0.16 (0.08)
	Extrinsic-only	0.22 (0.08)	0.14 (0.06)	0.15 (0.06)	0.16 (0.06)	0.12 (0.05)	0.11 (0.05)
FDP	Intrinsic	0.30 (0.25)	0.28 (0.24)	0.26 (0.22)	0.17 (0.09)	0.17 (0.08)*	0.16 (0.09)*
	Extrinsic-only	0.34 (0.24)	0.20 (0.12)	0.26 (0.20)	0.17 (0.11)	0.13 (0.05)	0.12 (0.05)
EDC	Intrinsic	0.24 (0.15)	0.22 (0.15)	0.23 (0.16)	0.22 (0.06)	0.12 (0.04)	0.12 (0.06)
	Extrinsic-only	0.44 (0.18)*	0.30 (0.10)	0.34 (0.17)*	0.20 (0.05)	0.11 (0.05)	0.10 (0.03)
EI	Intrinsic	0.58 (0.21)	0.52 (0.21)*	0.53 (0.21)*	0.25 (0.05)	0.12 (0.03)	0.12 (0.04)
	Extrinsic-only	0.59 (0.22)	0.40 (0.15)	0.48 (0.20)	0.22 (0.05)	0.14 (0.06)	0.13 (0.06)

* Significant difference between Intrinsic and Extrinsic-only models.

For static pressing tasks, there were differences between models for relative antagonist activity and normalized antagonist moment. The Intrinsic model had higher relative antagonist activity and normalized antagonist moment compared to the Extrinsic-only model ($F_{1, 9}$ = 93.99, $p < .001$). Relative antagonist activity was higher in the flexed postures compared to the extended posture ($F_{2, 18}$ = 8.316, $p = .003$) (Figure 4.4). Both relative antagonist activity and normalized antagonist moment increased at the highest pressing force ($F_{2, 18}$ = 3.873, $p < .040$) (Figure 4.5).

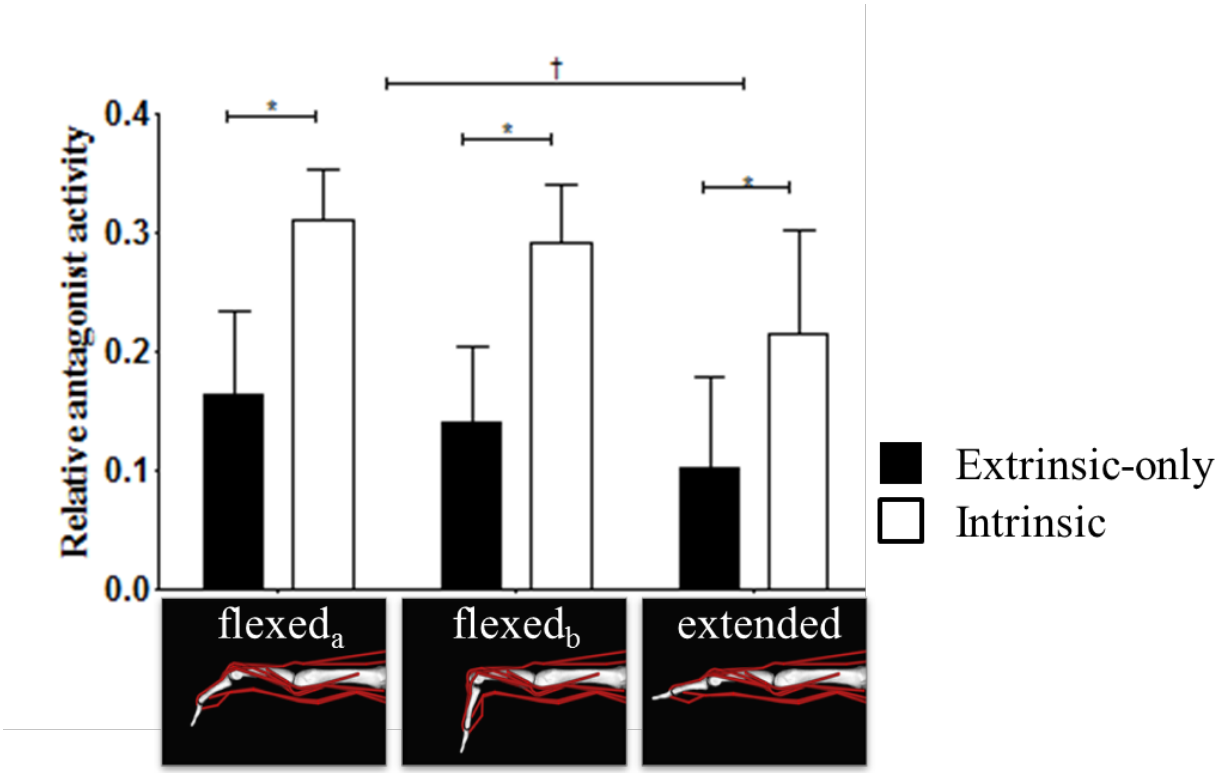

Figure 4.4 Mean relative antagonist activity for each model across static pressing postures. Data are collapsed across solutions methods. In flexed$_a$ both the PIP and DIP joint are bent, while in flexed$_b$ the DIP remains extended.
* Significant difference between Intrinsic and Extrinsic-only models.
† Significant difference between Flexed and Extended postures.

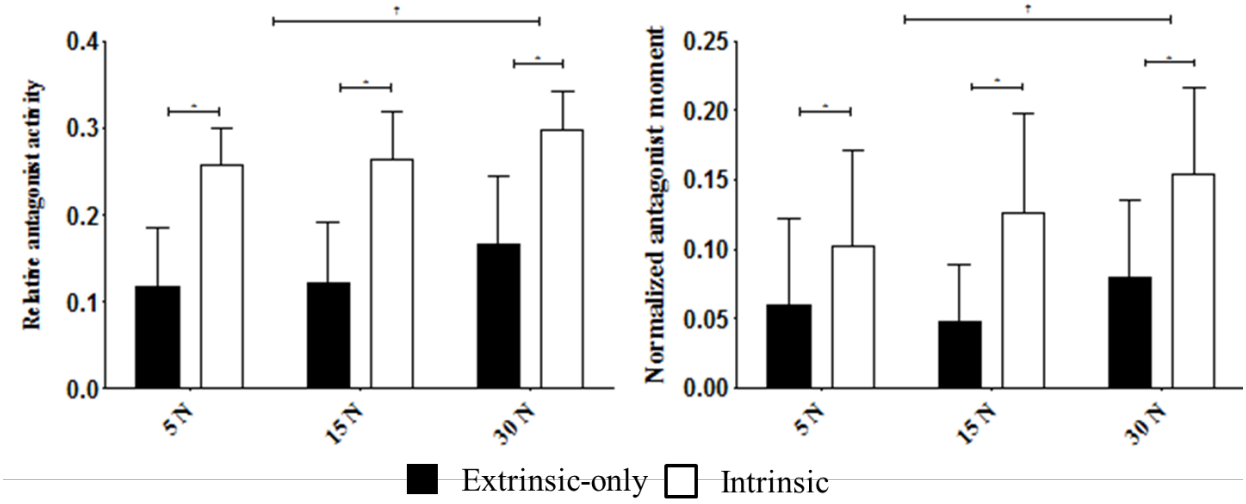

Figure 4.5 Mean relative antagonist activity (left) and normalized antagonist moment (right) for each model across static pressing forces. Data are collapsed across solution methods.
* Significant difference between Intrinsic and Extrinsic-only models.
† Significant difference between high and low forces.

4.2.3 Terminal slip versus central slip force distribution

Mean profiles of each dynamic task performed at fast and slow speeds can be found in Figures 4.6, 4.7. The accompanying descriptive statistics are presented in this section. The terminal slip to central slip force distribution averaged 0.60: 0.40, ± 0.06 across participants for slow tasks and 0.59: 0.41 ± 0.07 during fast tasks. Slip distribution changed by up to 20% throughout the cycle of each task, and varied more in slow trial than in fast. Slip force varied the most during slow tapping motions (range during one cycle = 0.17 ± 0.08) compared to when the finger was moving fast (range during one cycle = 0.09 ± 0.04). Slip distribution remained the most consistent throughout pointing and triggering tasks. During fast pointing cycles, the terminal slip contribution varied from 0.55 to 0.61 (range during one cycle = 0.06 ± 0.05) and during slow triggering cycles the terminal slip contribution varied from 0.54 to 0.59 (range during one cycle = 0.05 ± 0.04).

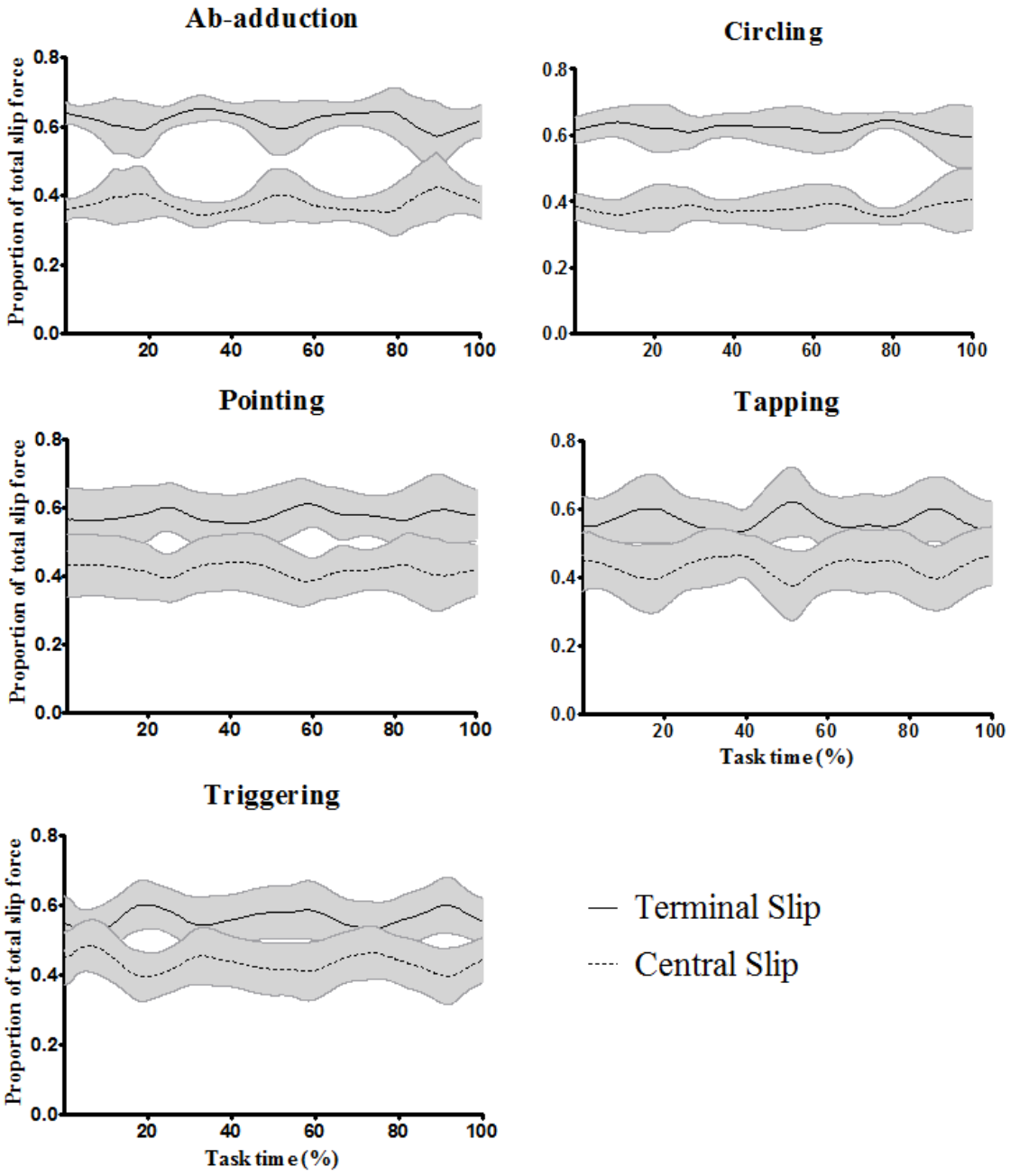

Figure 4.6 Mean terminal and central slip contribution (as a proportion of total force from both slips) during the five dynamic tasks when performed fast. Terminal slip (solid), central slip (dotted) and one standard deviation in grey.

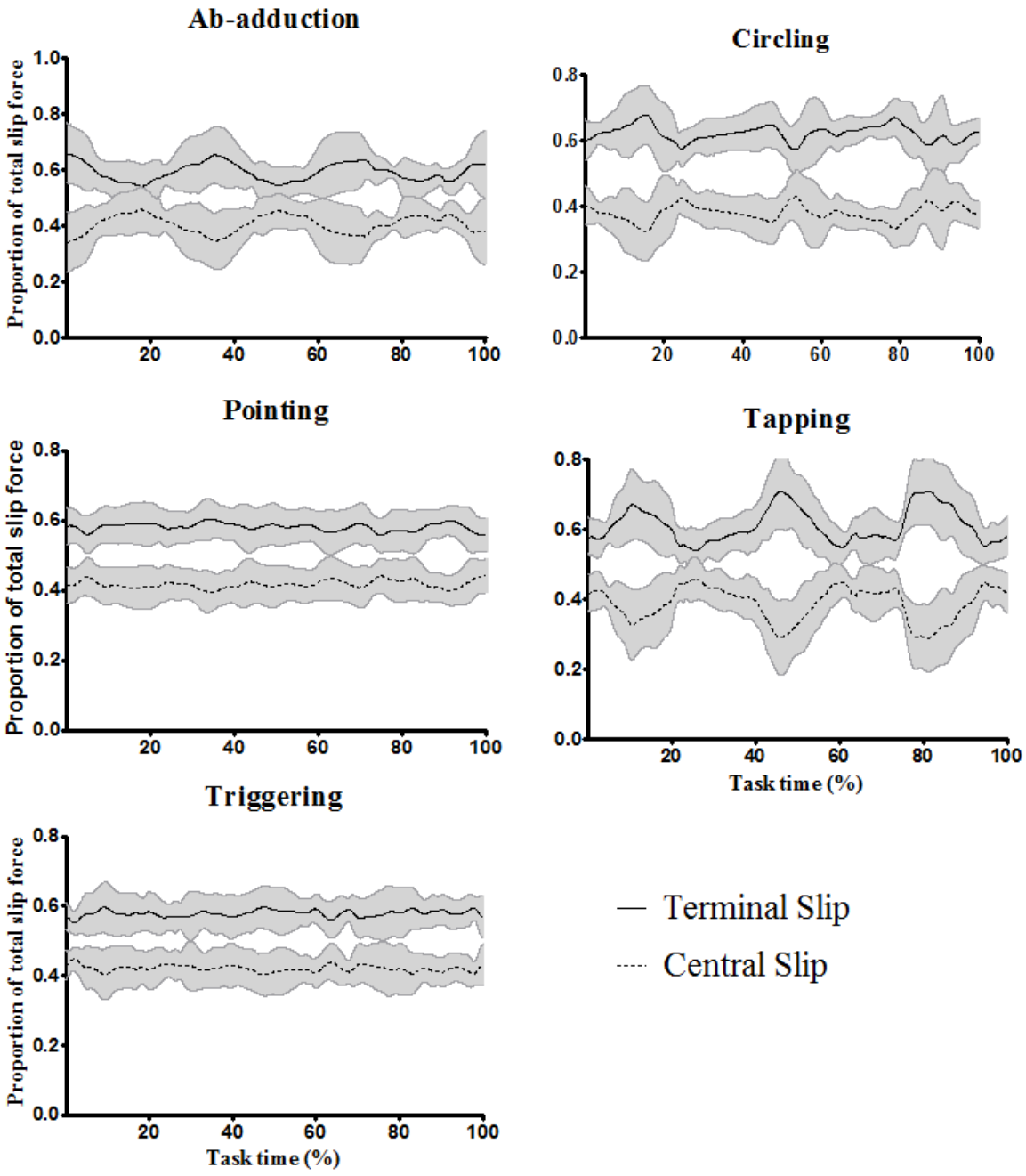

Figure 4.7 Terminal and central slip contribution (as a proportion of total force from both slips) during the five dynamic tasks when performed slow. Terminal slip (solid), central slip (dotted) and one standard deviation in grey.

For static pressing tasks, the average terminal slip to central slip force distribution (as a proportion of total slip force) was 0.59: 0.41, ± 0.05 across participants. Differences in slip distribution across posture and forces were assessed using EMG-constrained Entropy optimization method as it had the closest match with experimental muscle activity. Using this solution method, terminal slip contribution increased with pressing force from 0.58 ± 0.09 at 5 N to 0.68 ± 0.08 at 30 N) ($F_{2, 18} = 3.661$, $p < 0.046$) and remained consistent across postures ($F_{2, 18} = 0.140$, $p < 0.871$) (Table 4.4).

Table 4.4 Proportion of terminal slip force (terminal slip force / terminal + central slip force) during static pressing tasks by force and posture.

	$Flexed_a$	$Flexed_b$	Extended	
5 N	0.60 (0.09)	0.58 (0.06)	0.57 (0.16)	
15 N	0.62 (0.09)	0.63 (0.07)	0.61 (0.16)	*
30 N	0.65 (0.07)	0.69 (0.08)	0.70 (0.13)	

* Significant difference in terminal slip contribution to total slip force between 5 N and 30 N static pressing tasks across all postures.

CHAPTER 5

DISCUSSION

This thesis presented a model and solution methods in an open-source musculoskeletal modelling environment (OpenSim) that improves the anatomic fidelity of the finger. The Intrinsic model provided higher relative extensor activity and normalized extensor moments when compared to the Extrinsic-only model during static palmar pressing. Using an EMG-constrained solution with a static optimization procedure that incorporated co-contraction provided closer matches to experimental activity as seen by significantly lower error in static and dynamic tasks. The model and solution method are newly developed tools for the OpenSim platform and can serve as valuable resources for researchers looking to assess manual tasks.

5.1 Slip forces and tendon tensions

EMG-constrained entropy-assisted optimization gave the lowest error between predicted and experimental muscle activity, and so results from this method were used to analyze slip distribution. It was hypothesized that terminal and central slip tension ratios would be unique to force, posture, and movement. Force did have a greater effect as terminal slip contribution was consistent across postures but increased by 10% from 5 N to 30 N in static pressing. In dynamic trials, slip contribution varied more in slow trial than in fast, but was similar across motions. Static and dynamic tasks produced similar terminal to central slip force distributions. Terminal slip force averaged 60% of the total slip force in dynamic tasks, and 63% across static tasks. However, no changes in slip forces were observed between flexed and extended postures in static tasks (62% ± 23 in $flexed_a$, 63% ± 20 in $flexed_b$, and 62% ± 42 in extended postures). The great variability between participants illustrated the challenge in confidently determining the

relationship between the terminal and central slips (Valero-Cuevas et al., 2007). Anatomic variability, the differences between force transmission characteristics of each structure, and the many combinations available to estimate muscle loading all complicate the solution. There is a wide range of estimates in the literature. In a previous computational modelling investigation from Lee et al. (2008), the terminal: central slip force ratio during static pressing remained consistent across postures at approximately 1.7:1. Similarly, Valero-Cuevas et al. (2007) found a ratio of approximately 2:1 depending on the input muscle forces. In the same study, Valero-Cuevas et al. (2007) directly measured slip forces in a cadaver model. This experiment resulted in a ratio in the opposite direction, approximately 1:2 (terminal: central slip force distribution). To put results from this thesis into context, there was approximately a 1.5:1 terminal: central slip ratio across static and dynamic tasks.

The contribution of force from each muscle, to the two slips, has a critical impact finger movement and on static fingertip force generation (Balasubramanian et al., 2014). Lee et al. (2008) evaluated the changes in force between the terminal and central slip by looking at differences in deformations under an applied load in a cadaver study. While this work was technically challenging, it gave insight into how muscle forces propagate through the extensor mechanism. With the Intrinsic model, estimates of how muscle forces propagate can readily be obtained. The difference in force between components of the same muscle (i.e. the terminal and central components of the EDC) can be interpreted as the propagation of tension through the finger. For instance, across static pressing tasks, force from the central component of EDC (EDC_C) was approximately 2 times greater than the terminal components (EDC_R, EDC_U). From this, one may conclude that the EDC muscle loses force as it travels distally along the

finger, which would be in accordance with the cadaver experiment performed by Valero-Cuevas et al. (2007) that found over twice as much force at the central slip compared to the terminal slip.

There is a high degree of variability in muscle force estimates across the literature (Figure 5.1). Often the design, solution method, and the tasks differ between studies. In some cases, intrinsic muscle forces have been combined into a single parameter, making it impossible to discern the role of each muscle (Li et al., 2000; Fowler and Nicol, 2000; Weightman and Amis, 1982). Our results suggest that the total extrinsic flexor force (the combined force from FDP and FDS) was 4.2 times the externally applied load, while the extrinsic extensor force (force from EDC and EI) was 0.3, and an intrinsic force (from FDI, FPI, and LUM) was 1.7 times the externally applied load across postures and forces during static pressing. In comparison, Placet et al. (2012) estimated the same extrinsic extensor force (0.3), but higher extrinsic flexor force (5.1) and intrinsic force (2.8) by using a model of the hand that incorporated a mechanical link at the wrist. These results were obtained for a task that involved pressing with all four fingers, and used an optimization technique to minimize muscle stress. Conversely, Valero-Cuevas et al. (1998) found a higher extrinsic extensor force (1.1) and a similar intrinsic force (1.9), but a lower extrinsic flexor force (3.48). Valero-Cuevas et al. (1998) examined a 27 N static pressing task while the index finger was highly constrained in a flexed posture. The higher extensor forces may be attributed to how Valero-Cuevas et al. (1998) adjusted the model moment arms and PCSA to best match experimental EMG and contact forces. In terms of matching for posture and force, a more direct comparison can be made with work by Vigouroux et al. (2007) who also examined high force extended finger pressing using a combined EMG and optimization approach (Table 5.1). The two studies predicted similar FDP values (approximately 2.6 times the externally applied load), however Vigouroux et al. (2007) predicted half as much force from the

radial interosseous (FDI), 2.2 times the force from FDS, and 3.7 times more force from EDC. Vigouroux et al., (2007) evaluated static pressing using the middle finger as opposed to the index, as such the radial interosseous (FDI in the index finger) activity is expected to be lower given its larger size and greater role in the index (Infantolino and Challis, 2010). Additionally, EMG data were incorporated as an inequality constraint to the static optimization solution which led to increased FDS and EDC estimates.

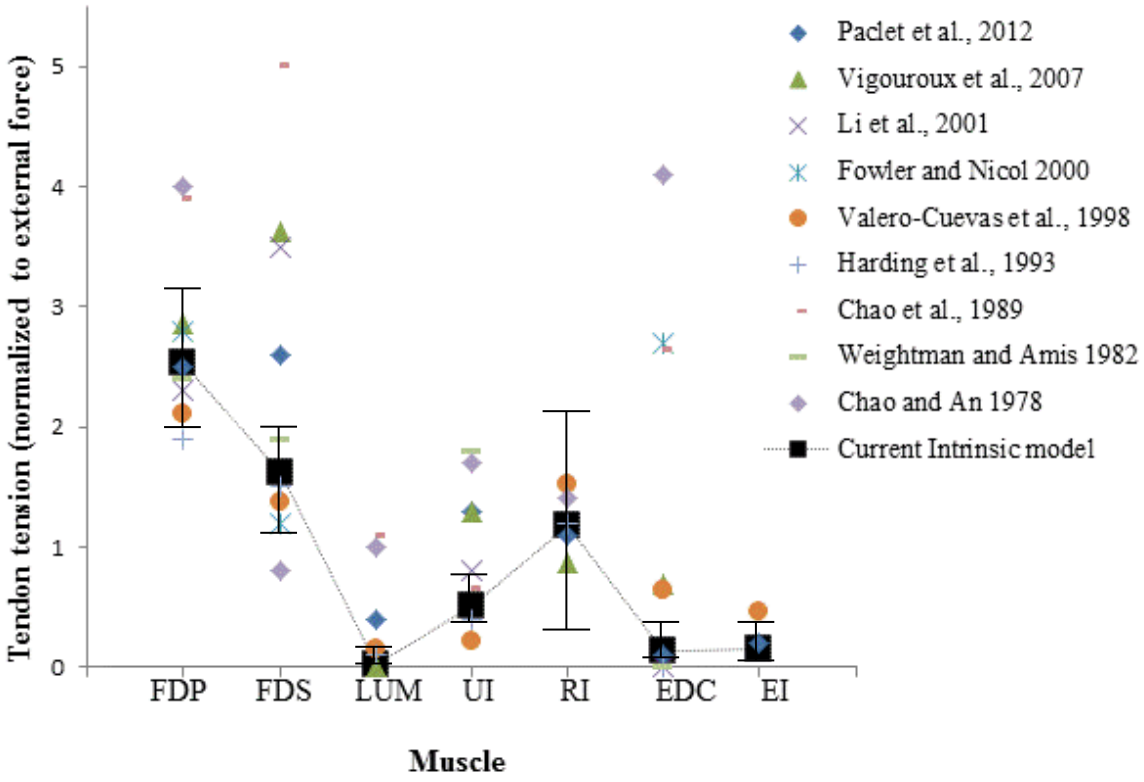

Figure 5.1 Muscle force estimates from literature compared with the current data (normalized to resultant external force). Range of data presented from this thesis are from all static palmar pressing trials. Radial interosseous (RI) corresponds to FDI and ulnar interosseous (UI) corresponds to FPI in the index finger.

Table 5.1 Tendon loading during extended finger static pressing at high force (normalized to resultant external force). (Actual LUM value for Intrinsic model = 0.004 (0.002)).

	FDP	FDS	LUM	UI	RI	EDC	EI
Vigouroux et al., 2007	2.85	3.62	0.00	1.29	0.88	0.68	-
Intrinsic model	2.66 (0.35)	1.64 (0.40)	0.00 (0.00)	0.41 (0.21)	1.76 (1.31)	0.18 (0.15)	0.18 (0.17)

5.2 Co-contraction in the finger

It was hypothesized that adding intrinsic muscles and a representation of the extensor mechanism would improve the fit and reduce the error between predicted and experimental muscle activities. There were no consistent overall differences in NRMSD and in r^2 between models and these results were specific to the solution method used. However, with the Intrinsic model we were able to address co-contraction in the finger. By assessing relative antagonist activity and normalized antagonist moment, the relationship between flexion and extension during static pressing could be captured. In the Extrinsic-only model, there was minimal relative antagonist activity and normalized antagonist moments. Using the Intrinsic model increased the predicted relative antagonist activity by 16%. This is a 29% improvement over to the Extrinsic-only model in relation to the relative antagonist activity calculated from experimental EMG. This increase in predicted antagonist activity is important since proper coordination depends on the relative flexor-extensor moments produced across the MCP, PIP, and DIP joints (Valero-Cuevas, 2005; Valero-Cuevas et al., 1998; Thomas and Long, 1968). Valero-Cuevas et al. (1998) had participants apply force from each side of their distal phalanx (palmar, dorsal, radial, ulnar, and tip). Muscle activity estimated from the model was able to elicit the required external force and matched experimental EMG for pressing in the palmar, dorsal, and distal directions.

From this result, the authors concluded that it was mechanically advantageous to use extensor muscles to produce palmarly directed external forces (Valero-Cuevas et al., 1998). This concept was further supported when Valero-Cuevas (2005) mathematically illustrated that, given the anatomical pathway of the musculature, co-contraction is necessary to be able to produce fingertip forces in all directions. In this thesis, normalized antagonist moments predicted from the Intrinsic model were 6 times greater than that from the Extrinsic-only model, without being constrained by EMG. This demonstrates that muscle pathways of the Intrinsic model facilitates a more appropriate distribution of forces required during static palmar pressing.

During static pressing, there were changes in relative antagonist activity at different postures but not for normalized antagonist moment. In the $flexed_a$ posture both the DIP and PIP joints were bent, while in the $flexed_b$ posture participants allow their DIP to extend. This difference caused an increase in PIP flexion angle in the $flexed_b$ posture. Moment arm has the largest effect in the $Flexed_b$ posture since PIP moment arm decreases with higher joint angles. The small extensor moment arms of the lateral bands at the PIP joint decreases the relative antagonist moment in the $Flexed_b$ posture (where the average PIP angle = 70° compared to 30° in the $flexed_a$ posture). However, activities from muscles attaching to the lateral bands are not mitigated by these small moment arms. As such, there is a change in mean activity across the three joints, but not in mean moment (Figure 5.2).

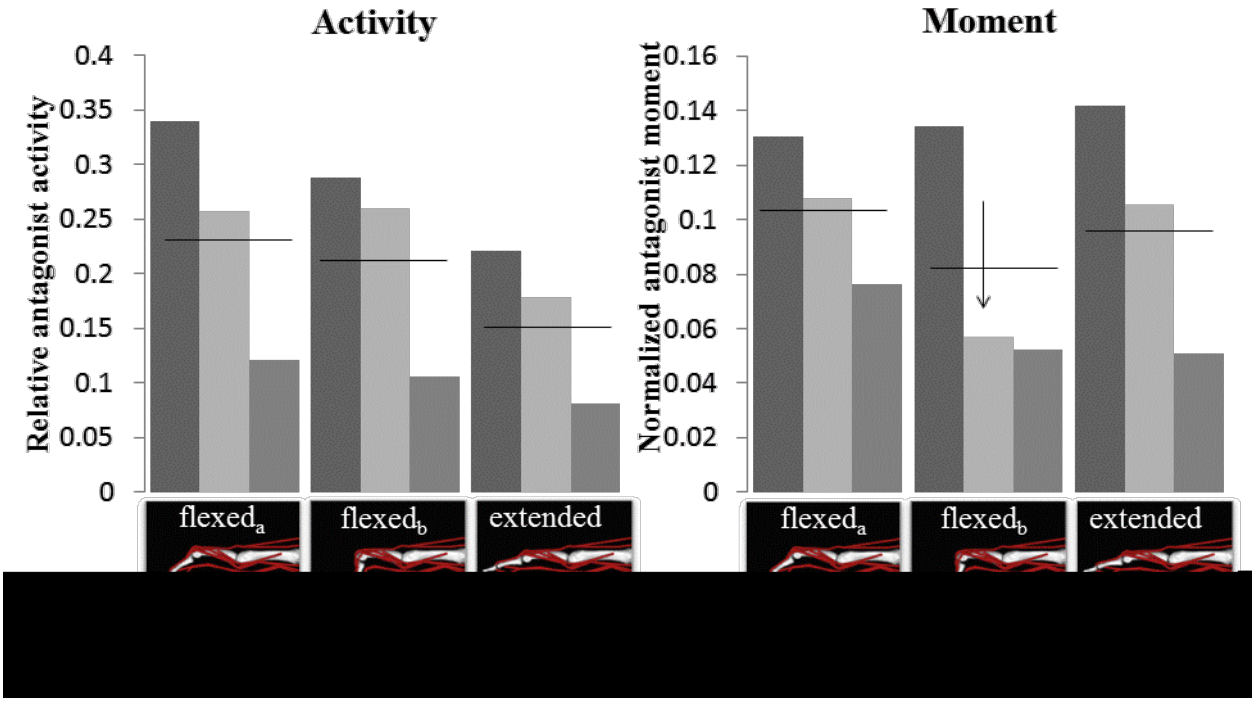

Figure 5.2 Relative antagonist activity at left (Equation 6 - sum of extensor activity/ sum of flexor and extensor activity for each joint) and normalized antagonist moment at right (Equation 7 - sum of extensor moments/ net joint moment) at each joint across pressing postures. Arrow above PIP moment in flexed$_b$ posture illustrates the difference between activity and moment that accounts for the mean postural affect observed across the finger for activity. Postural effect not observed for moment due to reduced lateral band extensor moment arms in high PIP flexion.

5.3 Solution method and muscle activity

In addition to the adjustments made to the model, the solution methods employed played an important role in the tendon tension distributions calculated. As hypothesized, using the Shift parameter and Entropy-assisted co-contraction objective functions provided lower error compared to the SSa objective across the range of static and dynamic tasks. Both co-contraction methods improve the prediction of antagonist activity, but the Entropy-assisted objective function gave a significantly lower NRMSD more frequently than the Shift parameter objective function. This supports the theory from the field of neurophysiology suggesting a weighted

balance between an agonist and antagonist drive (Lewis et al., 2010; Feldman, 1993; DeLuca and Mambrito, 1987). Parsa et al. (2013) examined these two objective functions with an unconstrained solution method using a planar model of the elbow. They found that the shift parameter and entropy-assisted objective functions provided similar trends in predicted antagonist activity. They also stated that the error between predictions from these methods and experimental results could be minimized by adjusting the objective function weight factor and shift parameter values. For this thesis, weight factors and shift parameter values were predetermined using a subset of data from one participant (Chapter 3.3.2).

As hypothesized, EMG-constrained methods did provide lower NRMSD and r^2 values than Optimization-only methods particularly for extensor muscles. Contrary to our hypothesis, the co-contraction objective functions did not improve the fit (r^2) with experimental data. In static pressing trials at high forces and in dynamic trials, EMG-constrained solutions using the SSa objective function provided higher r^2 values but also a larger errors between predicted and experimental results. Conversely, when using the co-contraction objective functions, there were smaller errors but also lower r^2 values. The ability of the co-contraction objective functions to predict more similar muscle activity is beneficial, particularly for static pressing tasks, as activity remained fairly consistent over the one second task. By more heavily constraining activity boundaries, r^2 values can be improved to match experimental activity for dynamic tasks. However this would restrict the freedom of the optimizer when finding appropriate forces for muscles that are not constrained by EMG.

5.4 Limitations

Forces from passive structures within the finger were not included in the current investigation. However, incorporating a viscoelastic tendon network in a musculoskeletal model is one of the largest challenges towards providing clinically relevant results (Valero-Cuevas, 2005). The influence of these structures is also variable. Qian et al. (2014) performed mechanical testing on 19 cadaveric extensor mechanisms. They found that thickness and strain were greater proximally. These variations in mechanical properties can have an influence on force transmission, and will be incorporated in future iterations of the model. The influence of passive structures also changes depending on speed of motion. During fast finger motions, muscle and ligament passive forces have been shown to have a significant effect. Sancho-Bru et al. (2001) simulated free motions with and without ligamentous forces. Their work demonstrates the need to incorporate passive properties in order to reproduce muscle force patterns during fast motions (Sancho-Bru et al., 2001, Sancho-Bru et al., 2003). Wohlman and Murray (2013) have added passive structures into a model of the thumb. They were able to reproduce experimentally derived contact forces using a forward dynamics approach. Muscle forces were determined using a Monte Carlo simulation across a wide range of muscle activities. While the results were specific to the task, they necessitate the incorporation of passive structures towards completing forward dynamic simulations that closely match experimental observations.

There are also important neurological and physical connections between fingers and between the hand and forearm that affect force transmission. These factors are not considered in the Intrinsic model. For example, the enslaving effect is characterized by involuntary movements or forces in fingers that are not associated with the voluntary movements or forces required to complete a particular task (Sanei and Keir, 2013; Schieber and Santello, 2004). The

enslaving effect is thought to derive from mechanical links between the extensor tendons of each finger and from neural restrictions between finger specific compartments of the extrinsic muscles (Leijnse et al., 2008; Keen and Fuglevand, 2004; Zatsiorsky et al., 2000). Forces from the extrinsic finger muscles also influence moments at the wrist. Placet et al. (2012) evaluated finger loading of two models, one that considers fingers independently, and one that has the fingers linked where balance at the wrist is accounted for. They found higher extensor tendon forces when the wrist is considered. They highlight the role of finger muscles towards balancing proximal moments. These factors indirectly influence tendon loading estimates of the index finger.

Providing a complete model of the hand, one that extends proximally would improve the anatomical fidelity and breadth of application for this model. The index finger alone was considered as an initial step. Computationally, it is expensive to run a complete analysis on the whole upper extremity in OpenSim. During preliminary testing, the Intrinsic model was appended to the whole Upper Extremity model (Holzbaur et al., 2005). A one second static optimization analysis with the whole upper extremity model took a prohibitively long time (after leaving it overnight, the analysis consistently would not begin to process. i.e. less than 1% complete). The wrap objects used to guide muscle paths can increase computational time (Christophy et al., 2012). Given the number of wrap objects in the whole model and the phantom limbs used in the Upper Extremity model (Holzbaur et al., 2005), it would be preferable to find an alternative method of setting muscle paths, possibly through using control point functions only (which are less expensive), and by appending the finger to the most recent dynamic model of the upper extremity released July 6, 2014 (Saul et al., 2014). These adjustments may allow the model to run more efficiently. The utility of the Intrinsic model is

limited to determining forces within the finger and does not account for more proximal interactions between fingers or at the wrist. This model should be incorporated into a model of the upper extremity to test how these interactions alter loading estimates in the finger.

For a third limitation, EMG was collected on the four extrinsic muscles and on FDI. Activity from FPI and LUM muscles were not collected and thus predicted activity of those muscles are dependent upon the objective criteria alone. Given the size and potential moments of these muscles it is possible that their contributions were underestimated. Physiologically, intrinsic muscles can provide fine motor control during manual tasks (Schroeder and Botte 2001; Ranney et al., 1988). The contribution from intrinsic muscles can be misleading when being evaluated with the current static optimization objective functions. While the co-contraction objective functions were used to increase antagonist activity, they do not incorporate principles of fine motor control. Alternative objective functions, such as those directed towards incorporating stability (Brown and Potvin, 2005; Cholewicki and McGill, 1994) may be able to alter the predicted activities for these muscles, but to our knowledge a static optimization objective function that preferentially activates smaller muscles has not been developed. A more appropriate option may be to direct efforts towards completing successful forward simulations that can accurately track desired kinematics and produces experimental end-point forces, while staying within the bounds of expected muscle activities. Results from these types of simulations would greatly improve the confidence of tendon loading distributions and predicted muscle activity for manual tasks.

As a final limitation, previous literature has demonstrated the sensitivity of predicted results to model and solution method parameters (Parsa et al., 2013; Valero-Cuevas et al., 1998). Many of these have been discussed (Section 3.3). In addition to these parameters, the EMG-

constraint value of ± 15% MVE was determined using a subset of static palmar pressing data ($flexed_a$ and extended postures at 5 and 30 N for one participant). Constraints from 5-25% were tested and 15% allowed the optimization to find a solution consistently, while also being able to observe the influence of both the constraint and the co-contraction objective functions. This constraint value has great influence of the NRMSD and r^2 values between predicted and experimental activity. A more tightly constrained solution would give a better fit and lower error, but would lead to the optimizer not being able to find a solution more frequently. If the constraint value were to increase or decrease, the findings presented in this thesis can be expected to hold true. In cases where experimental activity was less than 15% MVE, predicted activity from EMG-constrained solutions were still significantly higher than the unconstrained activity. In terms of getting predicted activity as close as possible to experimental recordings, the EMG-constraint value would need to be reduced. Alternatively, it may be useful for an EMG-assisted solution to be developed for OpenSim. This would incorporate experimental activity directly into the objective function. With this method, a closer match may be made between predicted and experimental activity and the optimizer would more consistently find a solution.

CHAPTER 6

SUMMARY AND FUTURE DIRECTIONS

6.1 Contributions

This thesis provides a way to evaluate tendon and joint loading through the finger for a variety of manual tasks. Towards this goal, a model of the index finger (The Intrinsic model) was developed that incorporates intrinsic muscles and the extensor mechanism. Additionally, new static optimization solution methods were programmed to compliment the model. This model and solution method can be used in the open-source musculoskeletal modelling platform, OpenSim. Data from this thesis indicate that, by using the Intrinsic model with the EMG-constrained co-contraction static optimization methods, tendon and joint loading estimates can be obtained that incorporate co-activation while maintaining mechanical equilibrium for static and dynamic tasks.

With this model, muscle contributions to joint loading can be readily discerned and analyzed. Being able to evaluate these muscle contributions has great clinical implications. Muscle damage or imbalance can cause finger impairment such as clawing and arthritis (Lee and Kamper, 2010; Valero-Cuevas et al., 2003; Brand and Hollister 1993; Leijnse, 1997). With the Intrinsic model we can estimate each muscles contribution to joint loading and provide evidence to develop clinical treatments towards regaining and maintaining proper hand function. Tendon transfer surgery technique can benefit from understanding how each muscle contributes to the production of force across the finger (Yamazaki et al., 2008; Tada et al., 1991). OpenSim has already been used to explore mechanical implants that interface with a transferred tendon to improve grip strength (Balsumaranian et al., 2013).

The Intrinsic model can also be helpful towards determining joint loading patterns to better understand joint dysfunction. For example, osteoarthritis (OA) is associated with higher internal joint loading (Lee and Kamper, 2010; Lewek et al., 2005). Work needs to be done to assess the mechanical pathways related to developing OA in the finger for the wide variety of tasks we can perform (Lee et al., 2014; Wu et al., 2012). Lee and Kamper (2010) showed that individuals with OA create higher co-contraction and joint forces at a lower external force compared to their healthy counterparts. The researchers collected extrinsic muscle EMG and grip force, and used a normative model of the finger to estimate muscle contributions to PIP joint force (Lee and Kamper, 2010). With the ability to evaluate joint loading during a variety of tasks, we can better understand the mechanical pathways by which injury and degradation occur. Additional clinical relevance for this work can be related to improving functional electrical stimulation techniques (Mansouri and Reinbolt, 2012; Crago et al., 1996). Functional electrical stimulation is designed to facilitate muscle innervations to complete a desired task. The muscle activity patterns identified from modelling the finger can help to predict the activity required to complete a manual task. By developing the Intrinsic model and static optimization analysis tool in OpenSim we have made future analyses and modelling manual tasks more accessible to the research community. By these means we are accelerating the discovery of principles related to control of the hand and providing evidence for intervention strategies to improve the quality of life for impaired populations.

6.2 Future directions

Modelling is a continuous and iterative process. Each step towards meaningful model predictions gains useful information and helps to identify critical components of a model or

solution method. Adding passive structures across each joint of the finger is a promising, immediate, and actionable step towards improving the Intrinsic model. Adding passive structures is likely to give activity estimates more similar to experimental observation, and can help towards assessing the model with a forward dynamics solution method (Wohlman and Murray, 2013; Valero-Cuevas 2005; Sancho-Bru et al., 2003; Knutson et al., 2000). The complete influence of passive structures across joint angles and velocities still needs to be clarified (Lee et al., 2014). Notwithstanding, passive forces can be considered from previous literature. After implementing these properties the experimental tasks can be re-analyzed and the model may be capable of performing forward dynamic simulations that match experimental observations.

In the long term, including the large anatomical and physiological differences between individuals would be beneficial. Patient specific modelling is one possible tool that can be used to address this variability and affect clinical outcomes. For example, patient specific measurements of the hip joint have been used to map differences in pressure related to the development of OA (Sánchez Egea et al., 2014). However, developing patient specific models can be arduous. Work is being done to improve this process. Patient specific parameters can be scaled to template meshes to adjust generic musculoskeletal models. The aim of this work is ultimately to image an individual (with CT, MRI, or other techniques) and apply that data to a generic musculoskeletal model such that theoretical treatments specific to that person can quickly be designed and improved upon (Fregly et al., 2012; Neal et al., 2009). While this work is useful for developing individual models, it still requires the collection of large data sets. Also, this method does not address the variability seen across the population and as such the breadth of the results is limited.

There is a need to capture population variability to accurately determine patterns in tendon and joint loading. Computational tools such as machine learning and probabilistic evaluation have been used to represent the variability seen in the population for different musculoskeletal parameters (Chopp-Hurley et al., 2014; Valero-Cuevas et al., 2009). These approaches can lead to important non-normally distributed parameter predictions that reflect the population variability. Additionally, distinct clusters of parameter values that satisfy a solution can be identified (Valero-Cuevas et al., 2009). Having clusters of likely parameters can be a compromise between the solutions from a generalized model (that may be less precise and not reflect any one individual) and solutions from patient specific models (that are highly accurate but are prohibitively expensive to implement on a large scale). Having groups of solutions allows researchers and clinicians to explore scenarios of control and rehabilitation that are more likely to represent specific populations, without having to collect large datasets.

6.3 Conclusion

This thesis presented model of the index finger with improved anatomical fidelity by including the intrinsic musculature and extensor mechanism of the finger. Muscle properties and paths were developed from the literature and match previously determined moment arms across the range of motion of each joint in the finger. To complement this model, a static optimization solution method that allows for EMG-constrained solutions and objective functions which incorporate co-contraction has also been developed. The Intrinsic model and newly applied solution methods have been tested across static and dynamic tasks at varying postures, forces, and speeds. We have improved predicted co-contraction known to be essential towards applying forces in different directions and maintaining finger posture. However, this are still gaps

between predicted and experimental activity which should be addressed in future research. The model and solution methods developed in this thesis are valuable resources for assessing manual tasks. By providing tendon loading and muscle activity estimates, rehabilitation and surgical strategies can be improved to enhance the quality of life for individuals who have a reduced ability to perform activities of daily living.

REFERENCES

1. Ait-Haddou, R., Jinha, A., Herzog, W., & Binding, P. (2004). Analysis of the force-sharing problem using an optimization model. Mathematical biosciences, 191(2), 111-122.

2. Amarantini, D., &Martin,L. (2004). A method to combine numerical optimization and EMG data for the estimation of joint moments under dynamic conditions. Journal of Biomechanics, 37(9), 1393-1404.

3. An, K. N., Chao, E. Y., Cooney, W. P., & Linscheid, R. L. (1985). Forces in the normal and abnormal hand. Journal of Orthopaedic Research, 3(2), 202-211.

4. An, K. N., Ueba, Y., Chao, E. Y., Cooney, W. P., & Linscheid, R. L. (1983). Tendon excursion and moment arm of index finger muscles. Journal of Biomechanics, 16(6), 419-425.

5. An, K.-N., Chao, E. Y., Cooney Iii, W. P., & Linscheid, R. L. (1979). Normative model of human hand for biomechanical analysis. Journal of Biomechanics, 12(10), 775-788.

6. Anderson, F. C., & Pandy, M. G. (2001). Dynamic optimization of human walking. Transactions-american society of mechanical engineers journal of biomechanical engineering, 123(5), 381-390.

7. Arnold, E. M., Ward, S. R., Lieber, R. L., & Delp, S. L. (2010). A model of the lower limb for analysis of human movement. Annals of Biomedical Engineering, 38(2), 269-279.

8. Balasubramanian, R., Montgomery, J., Mardula, K., & Allan, C. (2013). Implanted Miniature Engineering Mechanisms in Tendon-Transfer Surgery Improve Robustness of Post-Surgery Hand Function. Paper presented at the The 6th Hamlyn Symposium on Medical Robotics (in press).

9. Balasubramanian, R., & Santos, V. J. (2014). The Human Hand as an Inspiration for Robot Hand Development: Springer.

10. Beasley, R. (2003). Beasley's Surgery of the Hand. New York, New York: Thieme Medical Publishers.

11. Bigland-Ritchie, B., Kukulka, C. G., Lippold, O. C., & Woods, J. J. (1982). The absence of neuromuscular transmission failure in sustained maximal voluntary contractions. The Journal of physiology, 330(1), 265-278.

12. Brand, P., & Hollister, A. Clinical mechanics of the hand, 1993. Mosby Year Book, St Louis (MO).

13. Brook, N., Mizrahi, J., Shoham, M., & Dayan, J. (1995). A biomechanical model of index finger dynamics. Medical engineering & physics, 17(1), 54-63.

14. Brown, S., & Potvin, J. (2005) Constraining spine stability levels in an optimization model leads to the prediction of trunk muscle co-activity and improved predictions of spine compression. Journal of Biomechanics, 38(4), 745-754.

15. Buchanan, T. S., Lloyd, D. G., Manal, K., & Besier, T. F. (2004). Neuromusculoskeletal modeling: estimation of muscle forces and joint moments and movements from measurements of neural command. Journal of applied biomechanics, 20(4), 367.

16. Buchner, H. J., Hines, M. J., & Hemami, H. (1988). A dynamic model for finger interphalangeal coordination. Journal of Biomechanics, 21(6), 459-468.

17. Bureau of Labor, S. (2012). Nonfatal Occupational Injuries and Illnesses Requiring Days Away From Work, 2011: United States Department of Labor.

18. Chalfoun, J., Younes, R., Renault, M., & Ouezdou, F. B. (2005). Forces, activation and displacement prediction during free movement in the hand and forearm. Journal of Robotic Systems, 22(11), 653-660.

19. Challis, J., & Kerwin, D. (1993). An analytical examination of muscle force estimations using optimization techniques. Proceedings of the Institution of Mechanical Engineers, Part H: Journal of Engineering in Medicine, 207(3), 139-148.

20. Chao, E. (1989). Biomechanics of the hand a basic research study. Teaneck NJ: World Scientific Publishing.

21. Chao, E., & An, K. (1978). Determination of internal forces in human hand. journal of the engineering mechanics division, 104(1), 255-272.

22. Cholewicki, J., & McGill, S. M. (1994). EMG assisted optimization: a hybrid approach for estimating muscle forces in an indeterminate biomechanical model. Journal of Biomechanics, 27(10), 1287-1289.

23. Chopp-Hurley, J. N., Langenderfer, J. E., & Dickerson, C. R. (2014). Probabilistic Evaluation of Predicted Force Sensitivity to Muscle Attachment and Glenohumeral Stability Uncertainty. Annals of Biomedical Engineering, 1-13.

24. Christophy, M., Senan, N. A. F., Lotz, J. C., & O'Reilly, O. M. (2012). A musculoskeletal model for the lumbar spine. Biomechanics and modeling in mechanobiology, 11(1-2), 19-34.

25. Clavero, J. A., GolanÃ³, P., FariÃ±as, O., Alomar, X., Monill, J. M., & Esplugas, M. (2003). Extensor Mechanism of the Fingers MR Imagingâ€"Anatomic Correlation1. Radiographics, 23(3), 593-611.

26. Crago, P. E., Lan, N., Veltink, P. H., Abbas, J. J., & Kantor, C. (1996). New control strategies for neuroprosthetic systems. Journal of Rehabilitation Research & Development, 33(2), 158-172.

27. Darling, W. G., Cole, K. J., & Miller, G. F. (1994). Coordination of index finger movements. Journal of Biomechanics, 27(4), 479-491.

28. De Luca, C., & Mambrito, B. (1987). Voluntary control of motor units in human antagonist muscles: coactivation and reciprocal activation. J Neurophysiol, 58(3), 525-542.

29. Delp, S. L., Anderson, F. C., Arnold, A. S., Loan, P., Habib, A., John, C. T., . . . Thelen, D. G. (2007). OpenSim open-source software to create and analyze dynamic simulations of movement. Biomedical Engineering, IEEE Transactions on, 54(11), 1940-1950.

30. Delp, S. L., & Loan, J. P. (2000). A computational framework for simulating and analyzing human and animal movement. Computing in Science & Engineering, 2(5), 46-55.

31. Dennerlein, J. T., Diao, E., Mote Jr, C. D., & Rempel, D. M. (1998). Tensions of the flexor digitorum superficialis are higher than a current model predicts. Journal of Biomechanics, 31(4), 295-301.

32. Eladoumikdachi, F., Valkov, P. L., Thomas, J., & Netscher, D. T. (2002). Anatomy of the intrinsic hand muscles revisited part I. Interossei. Plastic and reconstructive surgery, 110(5), 1211-1224.

33. Eladoumikdachi, F., Valkov, P. L., Thomas, J., & Netscher, D. T. (2002). Anatomy of the intrinsic hand muscles revisited part II. Lumbricals. Plastic and reconstructive surgery, 110(5), 1225-1231.

34. Erdemir, A., McLean, S., Herzog, W., & van den Bogert, A. J. (2007). Model-based estimation of muscle forces exerted during movements. Clinical Biomechanics, 22(2), 131-154.

35. Feldman, A. (1993). The coactivation command for antagonist muscles involving Ib interneurons in mammalian motor control systems: an electrophysiologically testable model. Neuroscience letters, 155(2), 167-170.

36. Feldman, A., Adamovich, S., Ostry, D., & Flanagan, J. (1990). The origin of electromyograms—explanations based on the equilibrium point hypothesis Multiple muscle systems (pp. 195-213): Springer.

37. Fok, K. S., & Chou, S. M. (2010). Development of a finger biomechanical model and its considerations. Journal of Biomechanics, 43(4), 701-713.

38. Forster, E., Simon, U., Augat, P., & Claes, L. (2004). Extension of a state-of-the-art optimization criterion to predict co-contraction. Journal of Biomechanics, 37(4), 577-581.

39. Fowler, N. K., Nicol, A. C., Condon, B., & Hadley, D. (2001). Method of determination of three dimensional index finger moment arms and tendon lines of action using high resolution MRI scans. Journal of Biomechanics, 34(6), 791-797.

40. Fregly, B. J., Besier, T. F., Lloyd, D. G., Delp, S. L., Banks, S. A., Pandy, M. G., & D'Lima, D. D. (2012). Grand challenge competition to predict in vivo knee loads. Journal of Orthopaedic Research, 30(4), 503-513.

41. Gagnon, D., Larivière, C., & Loisel, P. (2001). Comparative ability of EMG, optimization, and hybrid modelling approaches to predict trunk muscle forces and lumbar spine loading during dynamic sagittal plane lifting. Clinical Biomechanics, 16(5), 359-372.

42. Garcia-Elias, M., An, K.-N., Berglund, L., Linscheid, R. L., Cooney Iii, W. P., & Chao, E. (1991). Extensor mechanism of the fingers. I. A quantitative geometric study. The Journal of hand surgery, 16(6), 1130-1136.

43. Goislard, d. M. B., Rossi, J. R. M., Berton, E., & Vigouroux, L. (2012). Quantification of Hand and Forearm Muscle Forces during a Maximal Power Grip Task. Medicine and science in sports and exercise.

44. Gonzalez, M. H., Mohan, V., Elhassan, B., & Amirouche, F. (2005). Biomechanics of the digit. Journal of the American Society for Surgery of the Hand, 5(1), 48-60.

45. Green, D. P., Hotchkiss, R. N., Pederson, W. C., Wolfe, S. W., & Roselius, E. (2005). Green's operative hand surgery.

46. Hamner, S. R., Seth, A., & Delp, S. L. (2010). Muscle contributions to propulsion and support during running. Journal of Biomechanics, 43(14), 2709-2716.

47. Harding, D. C., Brandt, K. D., & Hillberry, B. M. (1993). Finger joint force minimization in pianists using optimization techniques. Journal of Biomechanics, 26(12), 1403-1412.

48. Harris, C., & Rutledge, G. (1972). The functional anatomy of the extensor mechanism of the finger. The Journal of Bone & Joint Surgery, 54(4), 713-726.

49. Herzog, W., & Binding, P. (1994). Effects of replacing 2-joint muscles with energetically equivalent 1-joint muscles on cost-function values of non-linear optimization approaches. Human movement science, 13(5), 569-586.

50. Hicks, J. (2013). [OpenSim Support How static optimization works]. Web Page.

51. Hodder, J. N., & Keir, P. J. (2013). Obtaining maximum muscle excitation for normalizing shoulder electromyography in dynamic contractions. Journal of Electromyography and Kinesiology, 23(5), 1166-1173.

52. Holzbaur, K. R. S., Murray, W. M., & Delp, S. L. (2005). A model of the upper extremity for simulating musculoskeletal surgery and analyzing neuromuscular control. Annals of Biomedical Engineering, 33(6), 829-840.

53. Hughes, R. E., & Chaffin, D. B. (1988). Conditions under which optimization models will not predict coactivation of antagonist muscles. Journal of Biomechanics, 21(10), 862.

54. Hultborn, H., Lindström, S., & Wigström, H. (1979). On the function of recurrent inhibition in the spinal cord. Experimental Brain Research, 37(2), 399-403.

55. Humphrey, D. R., & Reed, D. J. (1983). Separate cortical systems for control of joint movement and joint stiffness: reciprocal activation and coactivation of antagonist muscles. Adv Neurol, 39, 347-372.

56. Infantolino, B. W., & Challis, J. H. (2010). Architectural properties of the first dorsal interosseous muscle. Journal of anatomy, 216(4), 463-469.

57. Jacobson, M. D., Raab, R., Fazeli, B. M., Abrams, R. A., Botte, M. J., & Lieber, R. L. (1992). Architectural design of the human intrinsic hand muscles. The Journal of hand surgery, 17(5), 804-809.

58. Jankowska, E., Padel, Y., & Tanaka, R. (1976). Disynaptic inhibition of spinal motoneurones from the motor cortex in the monkey. The Journal of physiology, 258(2), 467-487.

59. Jiang, Z., & Mirka, G. A. (2007). Application of an Entropy-Assisted Optimization Model in Prediction of Agonist and Antagonist Muscle Forces. Paper presented at the Proceedings of the Human Factors and Ergonomics Society Annual Meeting.

60. Jinha, A., Ait-Haddou, R., & Herzog, W. (2006). Predictions of co-contraction depend critically on degrees-of-freedom in the musculoskeletal model. Journal of Biomechanics, 39(6), 1145-1152.

61. Kamper, D. G., Fischer, H. C., & Cruz, E. G. (2006). Impact of finger posture on mapping from muscle activation to joint torque. Clinical Biomechanics, 21(4), 361-369.

62. Keen, D. A., & Fuglevand, A. J. (2004). Common input to motor neurons innervating the same and different compartments of the human extensor digitorum muscle. Journal of neurophysiology, 91(1), 57-62.

63. Keir, P. J., & Wells, R. P. (2002). The effect of typing posture on wrist extensor muscle loading. Human Factors The Journal of the Human Factors and Ergonomics Society, 44(3), 392-403.

64. Kellis, E., Arabatzi, F., & Papadopoulos, C. (2003). Muscle co-activation around the knee in drop jumping using the co-contraction index. Journal of Electromyography and Kinesiology, 13(3), 229-238.

65. Knutson, J. S., Kilgore, K. L., Mansour, J. M., & Crago, P. E. (2000). Intrinsic and extrinsic contributions to the passive moment at the metacarpophalangeal joint. Journal of Biomechanics, 33(12), 1675-1681.

66. Kociolek, A. M., & Keir, P. J. (2011). Modelling tendon excursions and moment arms of the finger flexors Anatomic fidelity versus function. Journal of Biomechanics, 44(10), 1967-1973.

67. Kursa, K., Diao, E., Lattanza, L., & Rempel, D. (2005). In vivo forces generated by finger flexor muscles do not depend on the rate of fingertip loading during an isometric task. Journal of Biomechanics, 38(11), 2288-2293.

68. Lacquaniti, F. (1992). Automatic control of limb movement and posture. Current opinion in neurobiology, 2(6), 807-814.

69. Landsmeer, J. (1955). Anatomical and functional investigations on the articulation of the human fingers. Acta anatomica.Supplementum, 25(24), 1-69.

70. Landsmeer, J. M. F. (1963). The coordination of finger-joint motions. The Journal of Bone & Joint Surgery, 45(8), 1654-1662.

71. Lee, S. W., Chen, H., Towles, J. D., & Kamper, D. G. (2008). Effect of finger posture on the tendon force distribution within the finger extensor mechanism. Journal of Biomechanical Engineering, 130(5), 051014.

72. Lee, S. W., & Kamper, D. (2010). Higher antagonist co-contraction in hand osteoarthritis leads to detrimental joint mechanics. Paper presented at the Proceedings of the 34th Annual Meeting of American Society of Biomechanics, Providence.

73. Lee, S. W., & Kamper, D. G. (2014). Transmission of musculotendon forces to the index finger The Human Hand as an Inspiration for Robot Hand Development (pp. 77-97): Springer.

74. Leijnse, J. (1997). Anatomical factors predisposing to focal dystonia in the musician's hand—principles, theoretical examples, clinical significance. Journal of Biomechanics, 30(7), 659-669.

75. Leijnse, J., Carter, S., Gupta, A., & McCabe, S. (2008). Anatomic basis for individuated surface EMG and homogeneous electrostimulation with neuroprostheses of the extensor digitorum communis. Journal of neurophysiology, 100(1), 64-75.

76. Lewek, M. D., Ramsey, D. K., Snyder-Mackler, L., & Rudolph, K. S. (2005). Knee stabilization in patients with medial compartment knee osteoarthritis. Arthritis & Rheumatism, 52(9), 2845-2853.

77. Lewis, G. N., MacKinnon, C. D., Trumbower, R., & Perreault, E. J. (2010). Co-contraction modifies the stretch reflex elicited in muscles shortened by a joint perturbation. Experimental Brain Research, 207(1-2), 39-48.

78. Li, Z. M., Zatsiorsky, V. M., & Latash, M. L. (2000). Contribution of the extrinsic and intrinsic hand muscles to the moments in finger joints. Clinical Biomechanics, 15(3), 203-211.

79. Lieber, R. L., Jacobson, M. D., Fazeli, B. M., Abrams, R. A., & Botte, M. J. (1992). Architecture of selected muscles of the arm and forearm anatomy and implications for tendon transfer. The Journal of hand surgery, 17(5), 787-798.

80. Maier, M. A., & Hepp-Reymond, M.-C. (1995). EMG activation patterns during force production in precision grip. Experimental Brain Research, 103(1), 108-122.

81. Mansouri, M., & Reinbolt, J. A. (2012). A platform for dynamic simulation and control of movement based on OpenSim and MATLAB. Journal of Biomechanics, 45(8), 1517-1521.

82. Marieb, E. N. (2003). Human anatomy and physiology (Vol. 6). San Francisco, CA: Pearson.

83. McDonald, A. C., Sanei, K., & Keir, P. J. (2013). The effect of high pass filtering and non-linear normalization on the EMG–force relationship during sub-maximal finger exertions. Journal of Electromyography and Kinesiology, 23(3), 564-571.

84. Millard, M., Uchida, T., Seth, A., & Delp, S. (2013) Flexing computational muscle: modeling and simulation of musculotendon dynamics. Journal of Biomechanical Engineering. 135 (2), 021005.

85. Neal, M. L., & Kerckhoffs, R. (2009). Current progress in patient-specific modeling. Briefings in bioinformatics, bbp049.

86. Nielsen, J., & Kagamihara, Y. (1993). The regulation of presynaptic inhibition during co-contraction of antagonistic muscles in man. The Journal of physiology, 464(1), 575-593.

87. Nikanjam, M., Kursa, K., Lehman, S., Lattanza, L., Diao, E., & Rempel, D. (2007). Finger flexor motor control patterns during active flexion An i in vivoi tendon force study. Human movement science, 26(1), 1-10.

88. Osu, R., Franklin, D. W., Kato, H., Gomi, H., Domen, K., Yoshioka, T., & Kawato, M. (2002). Short-and long-term changes in joint co-contraction associated with motor learning as revealed from surface EMG. Journal of Neurophysiology, 88(2), 991-1004.

89. Paclet, F., & Quaine, F. (2012). Motor control theories improve biomechanical model of the hand for finger pressing tasks. Journal of Biomechanics, 45(7), 1246-1251.

90. Palastanga, N. P., & Soames, R. (2011). Anatomy and human movement structure and function: Churchill Livingstone.

91. Parsa, B., Ehsani, H., & Rostami, M. (2013). Analyzing synergistic and antagonistic muscle behavior during elbow planar flexion-extension: Entropy-assisted vs. shift-parameter criterion. Paper presented at the Biomedical Engineering (ICBME), 2013 20th Iranian Conference on.

92. Potvin, J., & Brown, S. (2004). Less is more: high pass filtering, to remove up to 99% of the surface EMG signal power, improves EMG-based biceps brachii muscle force estimates. Journal of Electromyography and Kinesiology, 14(3), 389-399.

93. Qian, K., Traylor, K., Lee, S. W., Ellis, B., Weiss, J., & Kamper, D. (2014). Mechanical properties vary for different regions of the finger extensor apparatus. Journal of Biomechanics.

94. Qiu, D., Fischer, H. C., & Kamper, D. G. (2009, 2009). Muscle activation patterns during force generation of the index finger. Paper presented at the Engineering in Medicine and Biology Society, 2009. EMBC 2009. Annual International Conference of the IEEE.

95. Raikova, R. T., & Prilutsky, B. I. (2001). Sensitivity of predicted muscle forces to parameters of the optimization-based human leg model revealed by analytical and numerical analyses. Journal of Biomechanics, 34(10), 1243-1255.

96. Ranney, D., & Wells, R. (1988). Lumbrical muscle function as revealed by a new and physiological approach. The Anatomical Record, 222(1), 110-114.

97. Ranney, D. A., Wells, R. P., & Dowling, J. (1987). Lumbrical function interaction of lumbrical contraction with the elasticity of the extrinsic finger muscles and its effect on metacarpophalangeal equilibrium. The Journal of hand surgery, 12(4), 566-575.

98. Sánchez Egea, A. J., Valera, M., Parraga Quiroga, J. M., Proubasta, I., Noailly, J., & Lacroix, D. (2014). Impact of hip anatomical variations on the cartilage stress: A finite element analysis towards the biomechanical exploration of the factors that may explain primary hip arthritis in morphologically normal subjects. Clinical Biomechanics, 29(4), 444-450.

99. Sancho-Bru, J. L., Perez-Gonzalez, A., Vergara, M., & Giurintano, D. J. (2003). A 3D biomechanical model of the hand for power grip. Journal of Biomechanical Engineering, 125(1), 78-83.

100. Sancho-Bru, J. L., Perez-Gonzalez, A., Vergara-Monedero, M., & Giurintano, D. (2001). A 3-D dynamic model of human finger for studying free movements. Journal of Biomechanics, 34(11), 1491-1500.

101. Sancho-Bru, J. n. L., Mora, M. C., LeÃ³n, B. E., PÃ©rez-GonzÃ¡lez, A., Iserte, J. L., & Morales, A. (2012). Grasp modelling with a biomechanical model of the hand. Computer methods in biomechanics and biomedical engineering(ahead-of-print), 1-14.

102. Sancho-Bru, J. n. L., Perez-Gonzalez, A., Vergara, M., & Giurintano, D. (2003). A 3D biomechanical model of the hand for power grip. Journal of Biomechanical Engineering, 125(1), 78-83.

103. Sanei, K., & Keir, P. J. (2013). Independence and control of the fingers depend on direction and contraction mode. Human movement science, 32(3), 457-471.

104. Sartori, M., Reggiani, M., Farina, D., & Lloyd, D. G. (2012). EMG-Driven Forward-Dynamic Estimation of Muscle Force and Joint Moment about Multiple Degrees of Freedom in the Human Lower Extremity. PloS one, 7(12), e52618.

105. Saul, K. R., Hu, X., Goehler, C. M., Vidt, M. E., Daly, M., Velisar, A., & Murray, W. M. (2014). Benchmarking of dynamic simulation predictions in two software platforms using an upper limb musculoskeletal model. Computer methods in biomechanics and biomedical engineering(ahead-of-print), 1-14.

106. Schieber, M. H., & Santello, M. (2004). Hand function: peripheral and central constraints on performance. Journal of Applied Physiology, 96(6), 2293-2300.

107. Son, J., Hwang, S., & Kim, Y. (2012). A hybrid static optimisation method to estimate muscle forces during muscle co-activation. Computer methods in biomechanics and biomedical engineering, 15(3), 249-254.

108. Standring, S., Ellis, H., Healy, J. C., Johnson, D., Williams, A., Collins, P., & Wigley, C. (2005). Gray's anatomy the anatomical basis of clinical practice. American Journal of Neuroradiology, 26(10), 2703.

109. Tada, H., Hirayama, T., & Takemitsu, Y. (1991). Extensor tendon rupture after osteoarthrosis of the wrist associated with nonrheumatoid positive ulnar variance. Clinical orthopaedics and related research, 262, 141-147.

110. Thelen, D. G., & Anderson, F. C. (2006). Using computed muscle control to generate forward dynamic simulations of human walking from experimental data. Journal of Biomechanics, 39(6), 1107-1115.

111. Thelen, D. G., Anderson, F. C., & Delp, S. L. (2003). Generating dynamic simulations of movement using computed muscle control. Journal of Biomechanics, 36(3), 321-328.

112. Thomas, D. H., Long II, C., & Landsmeer, J. (1968). Biomechanical considerations of lumbricalis behavior in the human finger. Journal of Biomechanics, 1(2), 107-115.

113. Valero-Cuevas, F. J. (2005). An integrative approach to the biomechanical function and neuromuscular control of the fingers. Journal of Biomechanics, 38(4), 673-684.

114. Valero-Cuevas, F. J., Anand, V. V., Saxena, A., & Lipson, H. (2007). Beyond parameter estimation: Extending biomechanical modeling by the explicit exploration of model topology. Biomedical Engineering, IEEE Transactions on, 54(11), 1951-1964.

115. Valero-Cuevas, F. J., Johanson, M. E., & Towles, J. D. (2003). Towards a realistic biomechanical model of the thumb the choice of kinematic description may be more critical than the solution method or the variabilityuncertainty of musculoskeletal parameters. Journal of Biomechanics, 36(7), 1019-1030.

116. Valero-Cuevas, F. J., Venkadesan, M., & Todorov, E. (2009). Structured variability of muscle activations supports the minimal intervention principle of motor control. Journal of neurophysiology, 102(1), 59-68.

117. Valero-Cuevas, F. J., Yi, J.-W., Brown, D., McNamara, R. V., Paul, C., & Lipson, H. (2007). The tendon network of the fingers performs anatomical computation at a macroscopic scale. Biomedical Engineering, IEEE Transactions on, 54(6), 1161-1166.

118. Valero-Cuevas, F. J., Zajac, F. E., & Burgar, C. G. (1998). Large index-fingertip forces are produced by subject-independent patterns of muscle excitation. Journal of Biomechanics, 31(8), 693-703.

119. van Dieën, J. H., Cholewicki, J., & Radebold, A. (2003). Trunk muscle recruitment patterns in patients with low back pain enhance the stability of the lumbar spine. Spine, 28(8), 834-841.

120. Vigouroux, L., Quaine, F., Labarre-Vila, A., Amarantini, D., & Moutet, F. o. (2007). Using EMG data to constrain optimization procedure improves finger tendon tension estimations during static fingertip force production. Journal of Biomechanics, 40(13), 2846-2856.

121. Village, J., Rempel, D., & Teschke, K. (2005). Musculoskeletal disorders of the upper extremity associated with computer work A systematic review. Occupational Ergonomics, 5(4), 205-218.

122. von Schroeder, H. P., & Botte, M. J. (2001). Anatomy and functional significance of the long extensors to the fingers and thumb. Clinical orthopaedics and related research, 383, 74-83.

123. Weightman, B., & Amis, A. A. (1982). Finger joint force predictions related to design of joint replacements. Journal of Biomedical Engineering, 4(3), 197-205.

124. Wells, R. P., & Ranney, D. A. (1986). Lumbrical length changes in finger movement a new method of study in fresh cadaver hands. The Journal of hand surgery, 11(4), 574-577.

125. Winslow, J. (1732). Exposition anatomique de la structure du corps humain: Paris, G. Desprez, et J. Desessartz.

126. Wohlman, S. J., & Murray, W. M. (2013). Bridging the gap between cadaveric and i in vivoi experiments A biomechanical model evaluating thumb-tip endpoint forces. Journal of Biomechanics, 46(5), 1014-1020.

127. Wu, J. Z., An, K.-N., Cutlip, R. G., Krajnak, K., Welcome, D., & Dong, R. G. (2008). Analysis of musculoskeletal loading in an index finger during tapping. Journal of Biomechanics, 41(3), 668-676.

128. Wu, S., He, L., Li, J., Wang, J., & Wang, S. (2012). Visual display terminal use increases the prevalence and risk of work-related musculoskeletal disorders among Chinese office workers a cross-sectional study. Journal of occupational health, 54(1), 34-43.

129. Yamazaki, H., Uchiyama, S., Hata, Y., Murakami, N., & Kato, H. (2008). Extensor tendon rupture associated with osteoarthritis of the distal radioulnar joint. Journal of Hand Surgery (European Volume), 33(4), 469-474.

130. Zajac, F. E. (1988). Muscle and tendon properties, models, scaling, and application to biomechanics and motor control. Critical Reviews in Biomedical Engineering, 17(4), 359-411.

131. Zancolli, E. (1979). Structural and dynamic bases of hand surgery (Vol. 2nd): Philadelphia.

132. Zatsiorsky, V. M., Li, Z.-M., & Latash, M. L. (2000). Enslaving effects in multi-finger force production. Experimental Brain Research, 131(2), 187-195.

APPENDIX A
SUPPLEMENTARY DATA

Moment arms for each muscle path in the Intrinsic model are compared to literature moment arms across the range of motion for each degree of freedom of the finger (Figures A.1, A.2).

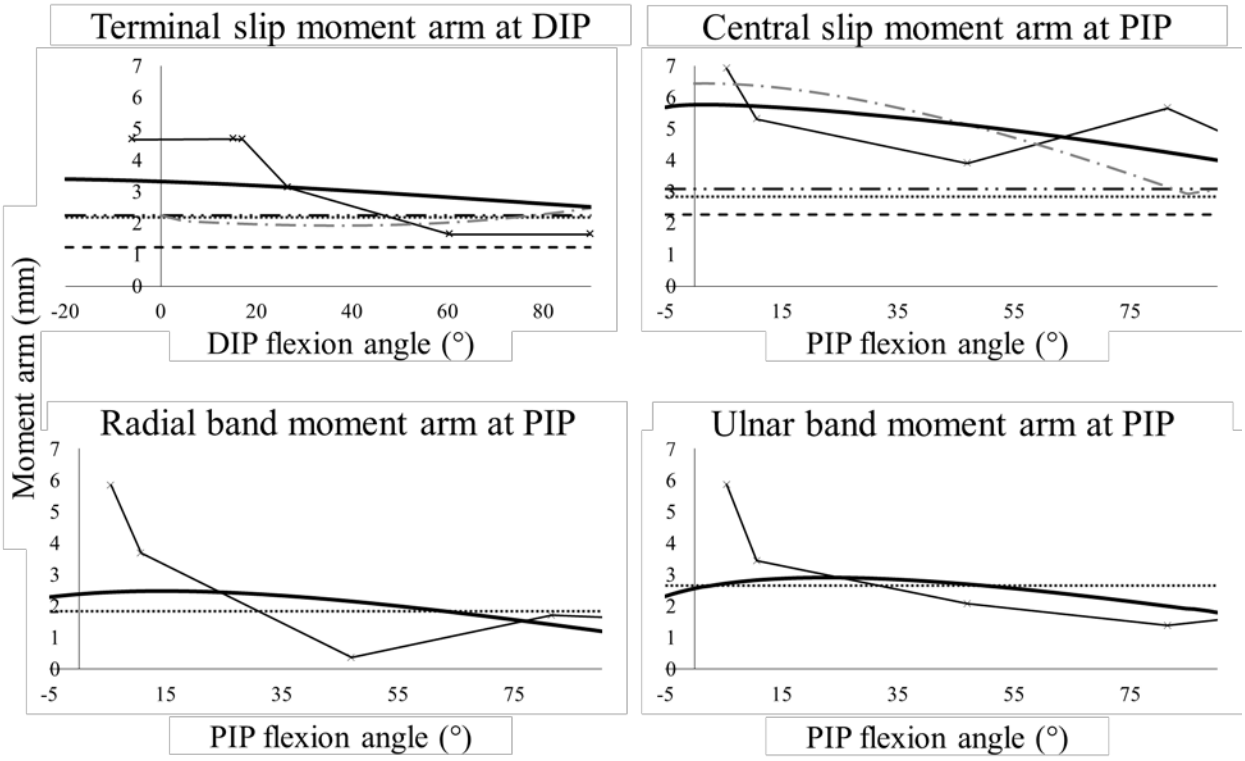

Figure A.1 Extension moment arms across the DIP and PIP joints compared to literature. Positive value indicates extension.

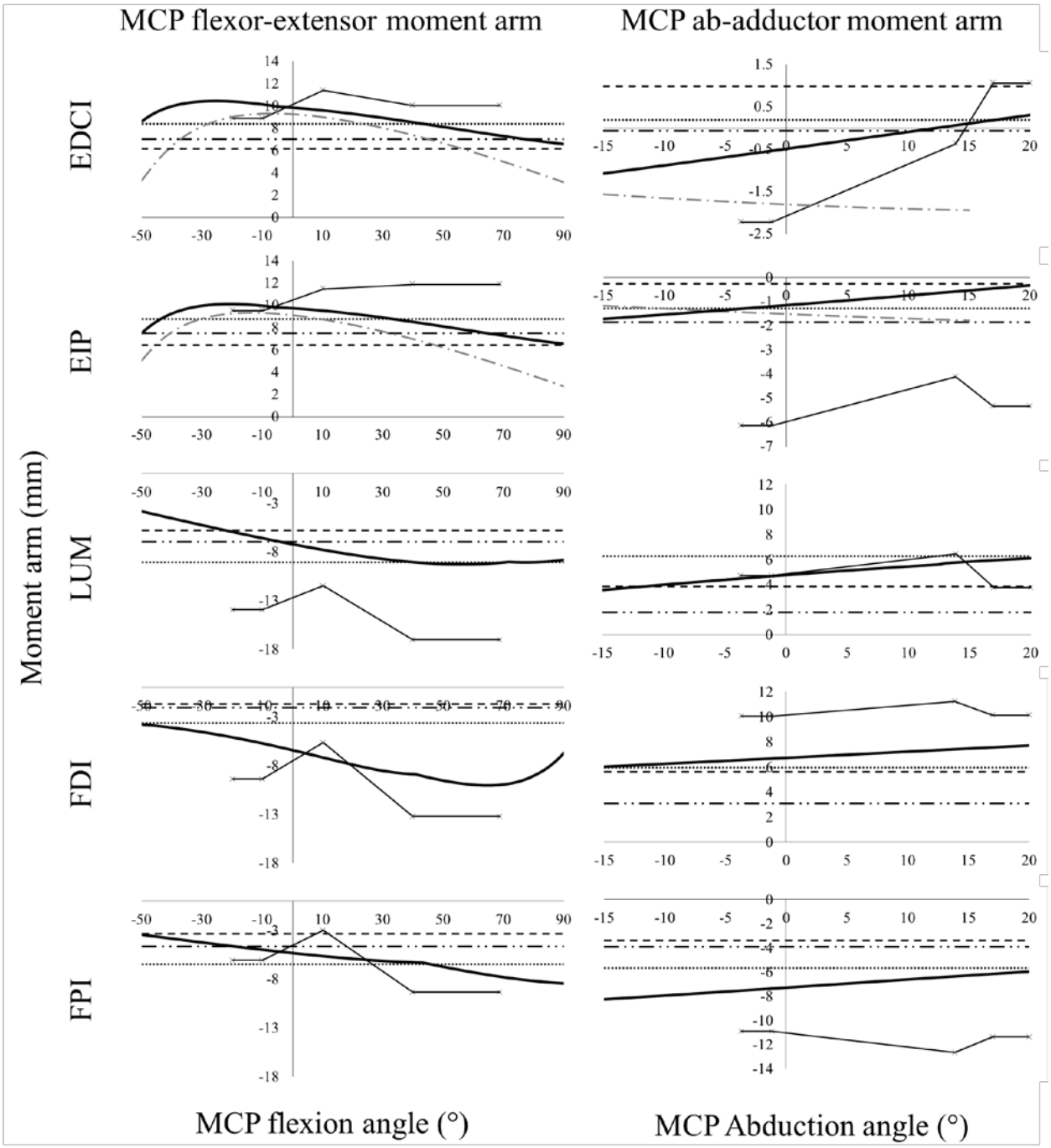

Figure A.2 Moment arms for each muscle across the MCP joint compared to literature. Positive values indicate extension and abduction.

Across participants, joint angles during static palmar pressing postures varied. However, the significant difference between PIP and DIP flexion-extension angles allowed for evaluations between postures.

Table A.1 Finger posture during static palmar pressing tasks. † Significant difference in PIP flexion-extension angle between each posture. ‡ Significant difference in DIP flexion-extension angle between Palmar Flexed$_a$ and other postures.

Posture	Mean joint angles (°)				Direction of pressing force
	MCP_FE	MCP_AB	PIP†	DIP‡	
Palmar Flexed$_a$	-3.1 (17.0)	9.5 (7.7)	30.7 (14.5)	33.8 (18.0)	Pressing down from the palmar side of the distal phalanx, perpendicular to the surface of the force cube
Palmar Flexed$_b$	1.1 (21.6)	11.3 (5.5)	71.6 (13.3)	-0.9 (20.9)	
Palmar Extended	-0.2 (22.2)	2.4 (11.9)	7.0 (2.7)	2.7 (17.2)	

The speed required during dynamic tasks was well met as it took participants an average of 5.86 ± 0.36 s to complete three cycles at the slow rate, and 1.98 ± 0.10 s at the fast rate. Table A.2 shows the average time to complete three cycles for each dynamic task.

Table A.2 Dynamic task average time to complete three cycles.

Task	Time to complete 3 slow cycles (s)	Time to complete 3 slow cycles (s)
Ab-adducting	5.83 (0.30)	1.96 (0.06)
Circling	5.85 (0.42)	1.94 (0.15)
Pointing	5.88 (0.69)	2.01 (0.10)
Tapping	5.89 (0.26)	2.00 (0.09)
Triggering	5.84 (0.11)	2.00 (0.09)

Table A.3 Significant findings from each ANOVA performed (Table 3.6). All significant main and interaction effects are identified here. Findings most relevant to the purposes of the thesis are highlighted in the results section 4.2.

ANOVA Type	Dependent variable	Significant finding	F statistic	Sig.
3x3x2x6 RM ANOVA Static pressing	NRMSD- FDP	Force	$F_{(1.02, 11.17)} = 7.431$	0.016
		Method	$F_{(1.04, 9.33)} = 6.493$	0.030
		Force*Model	$F_{(1.16, 10.46)} = 4.747$	0.049
	NRMSD- FDS	Method	$F_{(1.01, 9.91)} = 8.349$	0.015
		Force*Model	$F_{(1.16, 10.46)} = 7.112$	0.020
		Force*Method	$F_{(1.57, 14.10)} = 5.79$	0.019
	NRMSD- EDC	Force	$F_{(1.91, 17.22)} = 8.249$	0.003
		Method	$F_{(1.54, 13.90)} = 28.285$	0.001
		Force*Method	$F_{(2.62, 23.65)} = 4.329$	0.017
	NRMSD- EI	Force	$F_{(2, 18)} = 9.134$	0.002
		Model	$F_{(1, 9)} = 25.181$	0.001
		Method	$F_{(1.15,10.37)} = 21.101$	0.001
		Force*Method	$F_{(1.98,17.81)} = 4.224$	0.032
		Model*Method	$F_{(1.5, 13.52)} = 15.105$	0.001
		Force*Model*Method	$F_{(2.74, 24.7)} = 4.058$	0.020
3x3x2x6 RM ANOVA Static pressing	r^2- FDP	Force	$F_{(1.63, 14.71)} = 7.414$	0.008
	r^2- FDS	Force	$F_{(1.59, 14.32)} = 7.7$	0.008
		Method	$F_{(1.52, 13.64)} = 16.742$	0.001
		Force*Method	$F_{(3.28, 29.52)} = 5.297$	0.004
	r^2- EDC	Force	$F_{(1.98, 17.8)} = 6.981$	0.006
		Model	$F_{(1, 9)} = 6.952$	0.027
		Method	$F_{(1.72, 15.47)} = 8.407$	0.004
		Posture*Force*Model	$F_{(2.72, 24.46)} = 5.242$	0.007
		Force*Method	$F_{(3.68, 33.12)} = 2.926$	0.039
		Model*Method	$F_{(2.75, 24.71)} = 8.063$	0.001
	r^2- EI	Force	$F_{(1.94, 17.47)} = 8.228$	0.003

		Method	$F_{(1.48, 13.33)} = 9.241$	0.005
		Force*Method	$F_{(4.25, 38.28)} = 2.891$	0.032
5x2x2x6 RM ANOVA Dynamic tasks	NRMSD- FDP	Motion	$F_{(2.96, 26.63)} = 4.74$	0.009
		Model	$F_{(1, 9)} = 13.142$	0.006
		Method	$F_{(1.02, 9.22)} = 15.406$	0.003
		Motion*Method	$F_{(1.93, 17.34)} = 5.725$	0.013
		Speed*Method	$F_{(1.1, 9.9)} = 6.546$	0.027
		Model*Method	$F_{(1.85, 16.66)} = 11.699$	0.001
	NRMSD- FDS	Speed	$F_{(1, 9)} = 5.154$	0.049
		Model	$F_{(1, 9)} = 70.424$	0.001
		Method	$F_{(1.14, 10.26)} = 15.777$	0.002
		Motion*Model	$F_{(1.37, 12.3)} = 4.512$	0.045
		Model*Method	$F_{(5, 45)} = 25.909$	0.001
	NRMSD- EDC	Method	$F_{(5, 45)} = 29.585$	0.001
		Speed*Method	$F_{(1.21, 10.93)} = 15.971$	0.001
	NRMSD- EI	Motion	$F_{(4, 36)} = 4.788$	0.003
		Model	$F_{(1, 9)} = 48.978$	0.001
		Method	$F_{(1.04, 9.37)} = 28.584$	0.001
		Motion*Model	$F_{(2.64, 23.8)} = 3.437$	0.038
		Speed*Model	$F_{(1, 9)} = 8.662$	0.016
		Motion*Method	$F_{(2.3, 20.73)} = 3.943$	0.031
		Speed*Method	$F_{(1.32, 11.9)} = 8.083$	0.011
		Model*Method	$F_{(5, 45)} = 29.654$	0.001
		Motion*Model*Method	$F_{(2.79, 25.07)} = 3.569$	0.031
		Speed*Model*Method	$F_{(1.98, 17.83)} = 4.803$	0.022
5x2x2x6 RM ANOVA Dynamic tasks	r^2- FDP	Motion	$F_{(1.86, 16.73)} = 4.035$	0.040
		Speed	$F_{(1, 9)} = 19.589$	0.002
		Motion*Speed	$F_{(2.59, 23.32)} = 3.801$	0.028
		Speed*Method	$F_{(5, 45)} = 10.046$	0.001

	r^2- FDS	Speed	$F_{(1, 9)} = 20.05$	0.002
		Model	$F_{(1, 9)} = 9.251$	0.014
		Method	$F_{(5, 45)} = 2.783$	0.028
		Motion*Method	$F_{(4.71, 42.39)} = 3.221$	0.016
	r^2- EDC	Speed	$F_{(1, 9)} = 38.732$	0.001
		Model	$F_{(1, 9)} = 5.477$	0.044
		Method	$F_{(1.22, 10.97)} = 16.086$	0.001
		Motion*Speed*Model	$F_{(3.13, 28.18)} = 3.884$	0.018
		Speed*Method	$F_{(2.03, 18.23)} = 3.887$	0.039
		Model*Method	$F_{(2.67, 24)} = 17.46$	0.001
	r^2- EI	Method	$F_{(1.16, 10.45)} = 30.011$	0.001
		Motion*Method	$F_{(3.94, 35.43)} = 4.129$	0.008
		Speed*Method	$F_{(1.62, 14.55)} = 9.395$	0.004
		Motion*Speed*Model	$F_{(4.74, 42.68)} = 2.595$	0.041
		Model*Method	$F_{(2.12, 19.09)} = 8.744$	0.002
3x3x2x6 RM ANOVA Static pressing	Mean relative antagonist activity	Posture	$F_{(2, 18)} = 8.316$	0.003
		Force	$F_{(2, 18)} = 4.811$	0.021
		Model	$F_{(1, 9)} = 153.565$	0.001
		Method	$F_{(1.09, 9.81)} = 33.411$	0.001
		Posture*Method	$F_{(3.27, 29.46)} = 5.038$	0.005
		Force*Method	$F_{(2.85, 25.65)} = 12.516$	0.001
3x3x2x6 RM ANOVA Static pressing	Mean normalized antagonist moment	Force	$F_{(1.15, 10.36)} = 32.528$	0.001
		Model	$F_{(1, 9)} = 71.281$	0.001
		Method	$F_{(1.02, 9.21)} = 18.857$	0.002
		Force*Model	$F_{(1.19, 10.7)} = 84.144$	0.001
		Force*Method	$F_{(1.23, 11.07)} = 24.636$	0.001
		Model*Method	$F_{(1.33, 11.99)} = 20.514$	0.001
		Force*Model*Method	$F_{(2.43, 21.84)} = 21.822$	0.001

3x3 RM ANOVA Static pressing	Terminal slip contribution	Method Force*Method	$F_{(1.27, 11.47)} = 39.106$ $F_{(3.65, 32.81)} = 12.319$	0.001 0.001

APPENDIX B

LETTER OF INFORMATION AND CONSENT

February 24, 2014

Letter of Information and Consent

Collection of Wrist & Forearm Postures

Principal Investigator: Dr. Peter Keir

Department of Kinesiology, McMaster University

(905) 525-9140 ext. 23543 (pjkeir@mcmaster.ca)

Student / Co-Investigator Alex MacIntosh **(905) 525-9140 ext. 20175**

Research Sponsor: Natural Sciences and Engineering Research Council (NSERC)

Purpose of the Study

Carpal tunnel syndrome and other disorders of the upper extremity are common in repetitive jobs that use forceful efforts and awkward wrist postures. Research in our laboratory seeks to evaluate the risk of these injuries. To do assess hand and finger function, we often use computer models, or simulations, as part of this process we need to see how muscle activity changes with simple motions and tasks, like pinching. The purpose of this study is to monitor the motion of the wrist and fingers while performing simple motions and a pinching task, and to use the muscle activity data to drive a computer simulation of the hand.

Procedures involved in the Research

Before completing these tasks a number of reflective markers will be affixed to your hand and wrist using double-sided tape. Our camera system registers the locations of the reflective markers but will not capture your image like a regular camera. At the same time, we will place surface electrodes on the forearm and hand to measure muscle activity. These electrodes will only monitor the electrical activity of the muscle and will not transmit an electrical signal to the body. Surface electrodes are small self-adhesive pads with a conductive gel in the middle. The skin

over each muscle will be shaved and cleaned with alcohol. For this study, muscle activity from four muscles in the forearm that flex and extend the index finger, plus one muscle on the back of the hand that moves the finger sideways will be recorded using the surface electrodes. Once the electrodes are placed, in order for us to calibrate the sensors, we will ask you to contract each muscle by pressing your finger against a secure surface. You will be asked to move your right hand in a number of motions and perform a series of different types of grips and pinches using a force sensing device. Each action will be less than 10 s in total and your total time in the lab should be under 90 minutes.

Potential Harms, Risks or Discomforts: The data collection is brief and amounts to moving your wrist through its comfortable range of motion and pinching at relatively low levels, thus poses no additional risks beyond your normal daily activities. However it is important to recognize minor the potential discomforts that may occur:

1. You may experience mild discomfort or skin irritation from being shaved and cleansed in preparation for electrode placement. This is usually very mild and clear within 24 hours.
2. There may be discomfort in your forearm related to muscle soreness from performing maximal contractions. If muscle soreness does occur, it is usually very mild and should dissipate within 72 hours.

Potential Benefits: We hope create a detailed model of the hand for biomechanical and ergonomic assessment. The research will not benefit you directly but should help assess jobs in the future so that their injury risk is reduced.

Confidentiality: Your identity will be kept confidential and the data collected will be used for teaching and research purposes only. No videos or video images with any identifying marks will be used to present the data. The information directly pertaining to you will be secured in a locked cabinet or on a secure computer for a maximum of 15 years.

Participation: Your participation in this study is voluntary. If you agree to participate, you can decide to stop at any time, even after signing the consent form or part-way through the study, with no consequences to you.

Payment or Reimbursement: You will be paid $20 for participating in the study.

Information about the Study Results: You may obtain information about the results of the study by contacting Dr. Keir directly.

Information about Participating as a Study Participant:

If you have questions or require more information about the study itself, please contact Dr. Keir. This study has been reviewed and has received ethics clearance from the McMaster Research Ethics Board. If you have concerns or questions about your rights as a participant or about the way the study is conducted, you may contact:

McMaster Research Ethics Board Secretariat

c/o Office of Research Services

Telephone: (905) 525-9140 ext. 23142

E-mail: ethicsoffice@mcmaster.ca

CONSENT

I have read the information presented in the information letter about a study being conducted by Dr. Peter Keir and Alex MacIntosh of McMaster University. I have had the opportunity to ask questions about my involvement in this study, and to receive any additional details I wanted to know about the study. I understand that I may withdraw from the study at any time, if I choose to do so, and I agree to participate in this study. I have been given a copy of this form.

_____

Name and Signature of Participant